C.E. SACLAY
DSM

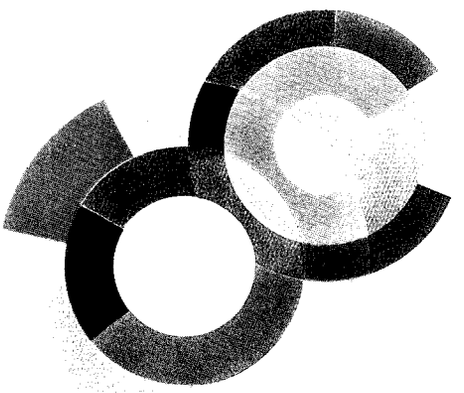

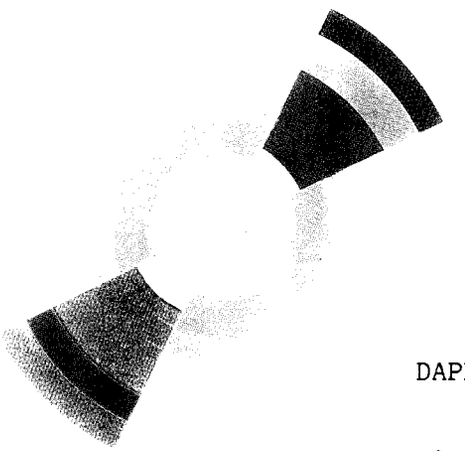

DAPNIA/SPhN 94 11 03/1994

^{3}H AND ^{3}He ELECTROMAGNETIC FORM FACTORS

A. Amroun, V. Breton, J.M. Cavedon,
B. Frois, D. Goutte, F.P. Juster,
Ph. Leconte, J. Martino, Y. Mizuno,
X.H. Phan, S.K. Platchkov, I. Sick,
S. Williamson

DAPNIA

Le DAPNIA (**D**épartement d'**A**strophysique, de physique des **P**articules, de physique **N**ucléaire et de l'**I**nstrumentation **A**ssociée) regroupe les activités du Service d'Astrophysique (SAp), du Département de Physique des Particules Elémentaires (DPhPE) et du Département de Physique Nucléaire (DPhN).

Adresse : DAPNIA, Bâtiment 141
CEA Saclay
F - 91191 Gif-sur-Yvette Cedex

Envoyé pour publication dans

Nuclear Physics A

^{3}H and ^{3}He electromagnetic form factors

A.Amroun [1], V. Breton [2], J.-M. Cavedon, B. Frois, D. Goutte,
F.P. Juster, Ph. Leconte, J. Martino, Y. Mizuno [3],
X.-H. Phan, S. K. Platchkov
DAPNIA/SPHN, C.E. Saclay, F-91191 Gif-sur-Yvette, France

I. Sick

Institut für Physik, Universität Basel,
CH-4056 Basel, Switzerland

S. Williamson
Dept.of Physics, University of Illinois, Urbana, USA

We report the results of three experiments on elastic electron scattering from ^{3}H and ^{3}He . A detailed description of the experiments and the data obtained is given. We have performed a combined analysis of the *world* data on ^{3}H and ^{3}He . This analysis gives a complete experimental information on the trinucleon electromagnetic form factors up to q^2=30 fm^{-2}, and also provides a separation into the isoscalar and isovector form factors. The results are compared to selected calculations that include nucleonic and mesonic degrees of freedom.

1 Introduction

The ground state wave functions of ^{3}He and ^{3}H nuclei can be accurately calculated from a realistic nucleon-nucleon interaction, including a consistent treatment of mesonic degrees of freedom. Calculations of the trinucleon ground state properties use either numerical solutions of the Faddeev equations, or variational methods. Both provide a solution of the Schödinger equation, for nonrelativistic nucleons bound by the nucleon-nucleon interaction. Important progress in the accuracy of these techniques has been achieved during the last decade. Today the binding en-

[1]Present address: Université d'Alger, Algerie
[2]Present address: Université de Clermont-Ferrand, France
[3]Present address: Dept. of Physics, Osaka University, Osaka, Japan

ergies, charge radii and electromagnetic form factors of the trinucleon systems have been computed with great accuracy by several groups [1, 2, 3, 4] and for a variety of two- and three-nucleon forces.

Three-nucleon wave functions are very sensitive to the choice of the nucleon-nucleon interaction, and the treatment of meson exchange currents and relativistic corrections. Therefore it is important to probe their shape in detail, in order to test the limits of our understanding of nuclear structure. Electromagnetic form factors provide the most detailed experimental information on these wave functions. Electron scattering data have shown that the nucleonic degrees of freedom alone can not explain the magnetic or the charge form factors. Two-body currents as well as relativistic effects have to be taken into account to get satisfactory agreement with the data.

Experimental studies of the electromagnetic structure of ^{3}He and ^{3}H have started in Stanford [5] three decades ago. The pioneering experiment by Collard *et al* measured the charge and magnetic form factors for both ^{3}He and ^{3}H. Since the momentum transfers were limited to 8 fm^{-2} no diffraction structure was observed. Because of the difficulty in dealing with radioactive tritium targets, only the ^{3}He nucleus was investigated in the following two decades. Its magnetic and charge form factors were measured up to 14 and 20 fm^{-2} respectively by McCarthy *et al* [6] and later extended to 75 fm^{-2} in an experiment by Arnold *et al* [7]. These experiments have shown important differences between experimental and theoretical form factors. During the last years much effort has been spent to measure data with improved accuracy. The low momentum transfer region was covered by Szalata *et al* [8], Ottermann *et al* [9] and Dunn *et al* [10], while the high-momentum part of the magnetic form factor was measured by Cavedon *et al* [11]. Studies of the tritium nucleus have been performed by Juster *et al* [12] and Beck *et al* [13]. The former has allowed to map out the diffraction structure of both the charge and magnetic form factors. Finally, the knowledge of the ^{3}He charge form factor was significantly improved in a very recent experiment in the q-region of the diffraction feature by Amroun *et al* [14].

All the trinucleon form factors are now accurately known up to momentum transfers q^2 of the order of 30 fm^{-2}, transfers large enough to cover the region of the secondary diffraction maximum. These data are now adequate for an detailed comparison with the most complete theoretical calculations including nucleonic and mesonic degrees of freedom. Since the experimental data on the ^{3}He and ^{3}H form factors now reach similar values of q^2, this comparison can be extended to the combinations of isospin T = 0 and T = 1, thus allowing a direct confrontation with form factors for the 2- and 4-body systems. These include the deuteron charge and magnetic form factors which are both pure T = 0 transitions, and deuteron electrodisintegration at threshold and backward angle, which is a magnetic T = 1 transition.

The purpose of this paper is to describe the three different experiments on ^{3}He and ^{3}H performed at Saclay [11, 12, 14], and to give a complete list of the experimental cross sections and form factors. In the first of these experiments, we have measured the ^{3}He magnetic form factor to larger q. The second experiment dealt with the charge and magnetic form factors of ^{3}H . In the last experiment, we improved the accuracy of the data for the charge form factor of ^{3}He . Preliminary results were already published. In order to provide the most complete experimental information on the form factors, we here also present a combined analysis of the world data for the A=3 nuclei. We conclude by a comparison of the form factors deduced with some of the most complete theoretical calculations now available.

2 Experimental set-up

The three experiments discussed below were performed using the electron scattering facility at Saclay [15].

2.1 Beam

The experiments made use of the 700 MeV electron linac, which provided a 500 Hz, 10 μsec pulsed electron beam. The data were taken in the HE1 experimental hall.

[15]. The incident beam was deflected into the HE1 hall by two 45° dipole magnets. Its energy spread was chosen using the energy-defining slits located halfway between the dipoles. A quadrupole, also located between the two dipoles, served to tune the dispersion due to the bending magnets as required: in the *achromatic* mode, the quadrupole compensated for the energy dispersion of the beam, in the *energy loss* mode it increased the dispersion by a factor of two, in order to match it at the target to the spectrometer dispersion.

In the energy loss mode, the transport system made use of a set of 5 quadrupoles which rotated the dispersion plane by 90° to allow for a compensation of switchyard and spectrometer energy dispersion. This rotator was used only for the experiment on the ^{3}He charge form factor. For the two other experiments achromatic beams were used, with a typical energy spread of $\Delta E/E = 10^{-3}$. The beam position was carefully adjusted using removeable view screens and two sets of steering coils. In addition, two quadrupoles allowed to focus the beam onto the target. The beam intensity was measured both with non-intercepting ferrite toroid monitors, and with a Faraday cup. A continuous comparison between these two measurements allowed an accurate monitoring of the number of incident particles.

During the experiment, the beam position was continuously controlled using a split secondary emission monitor placed downstream of the target. Its signals were used to stabilize the beam position using a separate set of steering coils.

The electron beam energy was varied from 189 MeV to 689 MeV depending on the kinematic conditions required. The beam intensity I was limited to the maximum values allowed by the particular target used. During the tritium experiment the limitation was set to 15 μA, mainly for safety reasons. Values of I up to 40 and 20 μA were used during the measurements of the magnetic and charge form factors of ^{3}He , respectively. Details on the targets are given below.

2.2 Electron detection

The scattered electrons were analyzed in the "900" magnetic spectrometer which deflected the electrons vertically and had a slit-defined aperture with a well known solid angle. The electrons were detected with a detection system consisting of two rows of plastic scintillators, a gas Cerenkov counter and two multiwire vertical drift chambers. Each chamber had two planes of active wires, with wires oriented horizontally, and wires inclined relative to them by 29°. The distance between the active wires was 6 mm. The chambers [16] were filled with a mixture of 50% argon–50% isobutane. Their midplanes were inclined by 39° relative to the mean electron trajectory, so at least 3 wires per plane were hit. For each event, the wire addresses and the corresponding drift times were recorded. This information was used to determine the coordinates where the scattered electron crossed the four wire chamber planes.

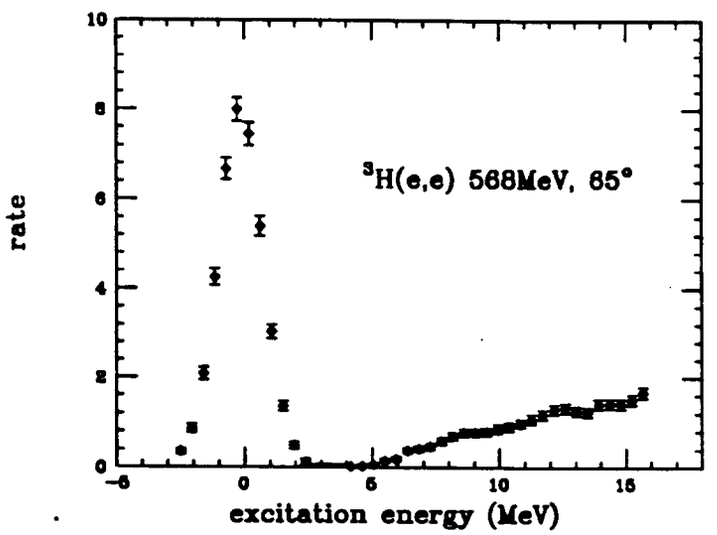

Figure 1: Energy spectrum of electrons of 568 MeV scattered by 65° for ^{3}H ; radiative effects have already been unfolded.

The four coordinates measured were then transformed into two angles and two focal plane coordinates. These quantities were used to perform an online trajectory reconstruction in order to determine the scattering angle and the location of the

interaction vertex within the target. The uncertainties of these determinations were $\pm$ 7 mrad, and $\pm$ 1 mm in a plane perpendicular to the midplane of the spectrometer. This knowledge allowed to minimize the uncertainty in the energy loss in the target, and allowed to partially correct for recoil energy differences which were important when the large spectrometer solid angles were used. For all experiments an overall resolution of the order of 2 MeV or better was achieved, leading to a clean separation of the elastic peak from the two-body break-up threshold. A typical spectrum is shown in figure 1.

2.3 Targets

The design of a tritium target containing of the order of 370 TBq (10000 curies) of ^{3}H required a thorough study of options and safety considerations.

We have chosen to use a target containing *liquid tritium*, as only this option provided the luminosity required to reach momentum transfers beyond the expected diffraction features in F_{ch} and F_m. For reasons of safety, we have designed a *sealed* cryogenic system that allowed to liquefy ^{3}H without any radioactive gas handling, except for the initial fill and final gas recuperation, carried out in specialized laboratory. Again for safety reasons, the tritium target was enclosed in three further sealed containers with thin windows for the electrons, and a massive container closed during transportation of the target. The general layout of the target is shown in figure 2.

The ^{3}H -target proper consisted of a stainless steel cylinder, 40 mm long, 10 mm in diameter with hemispherical end caps. The wall thickness of the cylinder was 0.5 mm. The thickness of the end caps varied between 0.5 and 0.05 mm from the edge to the axis of the target. The end caps were located outside the acceptance of the spectrometer. At our extreme angle of 155°, they were shielded by an additional collimator (see below). The calculated bursting pressure of the target was 110 bars. Destructive tests of similar cells lead to bursting pressures that were in agreement with the calculation.

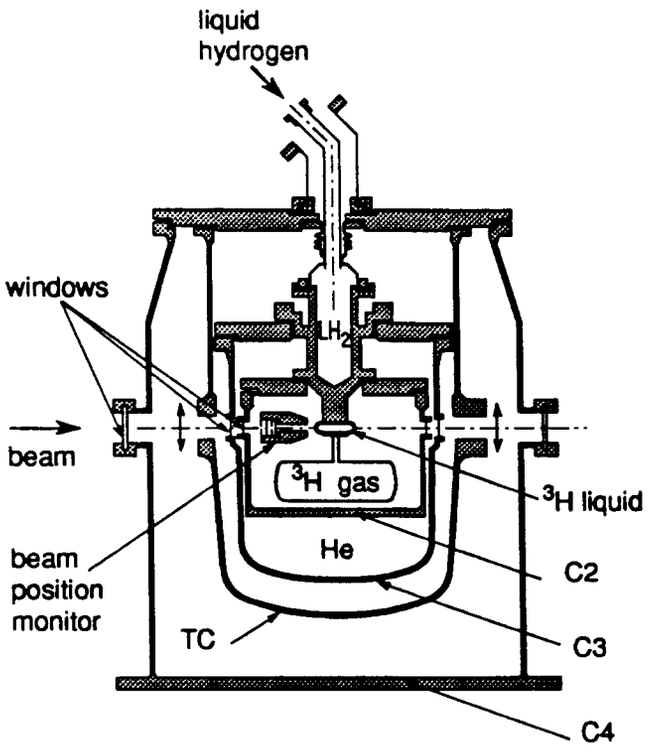

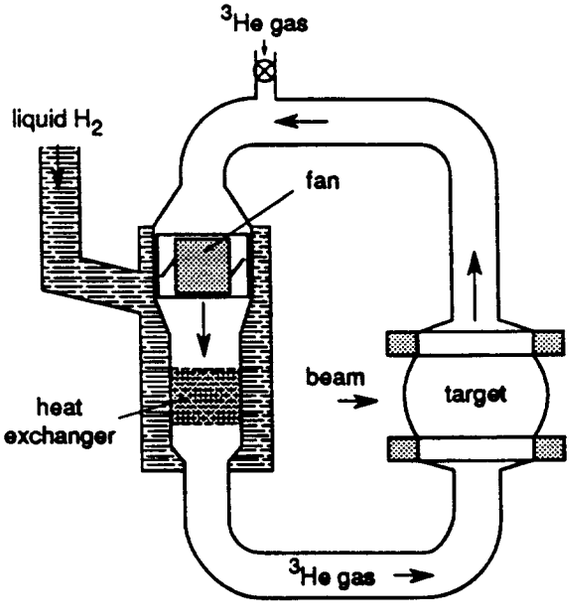

Figure 2: Tritium and Helium targets.

The target was in permanent connection with an expansion-vessel of 180cm^3 volume. This vessel was equipped with a heater, in order to keep it at T $\sim$ 300K while the target was cold. When the entire system was at room temperature, the tritium pressure was 23 bars, *i.e.* far below the allowed maximum pressure.

This combination of cold target and warm storage vessel had a number of outstanding benefits, such as high target density (liquid ^{3}H), low operating pressure (3 bars) while the target was placed in the high-intensity electron beam, very high efficiency in the use of the ^{3}H (98% in the cold target cell), well known density of liquid ^{3}H , and thin target windows.

Cooling was achieved by keeping the target in contact with a reservoir filled with liquid hydrogen, the reservoir and connection to the target being made of massive pure copper(OFHC). The copper actually covered about 80% of the circumference of the target cylinder, leaving open only the solid angle towards the 900 spectrometer. This arrangement ensured optimal thermal contact between the liquid ^{3}H and the LH_2-reservoir.

The target and ^{3}H storage vessel were enclosed in three additional containers, C2, C3, C4. These containers were permanently sealed, and had stainless steel windows for the incoming and outgoing beam, and scattered electrons (0.01 to 0.05 mm thick). Volume V_2 (defined by container C2) was evacuated with a permanently operating getter pump, and was designed to retain, in case of a failure of the ^{3}H -target, the tritium at a pressure *below* atmospheric pressure (0.6 bar). Volume V3 (defined by containers C2 and C3) was filled with gaseous ^{4}He at 0.8 bar pressure. Volume V4, defined by C3 and the standard scattering chamber equiped with permanent stainless steel windows for beam and scattered electrons, was evacuated.

The gaseous ^{4}He in volume V3 had the purpose of checking continuously the integrity of containers C2 and C3; loss of integrity would result in a decrease of the pressure of ^{4}He in C3, and the appearance of ^{4}He in C2 or C4, containers that both were equipped with a small residual-gas mass spectrometer. As a matter of fact, during operation of the target in a high-intensity beam, the containers C2 and C3 — the windows of which were not cooled — were punctured by a beam that was

grossly overfocused. The detection of ^{4}He in C2, C4 led to an orderly shutdown of the experiment, with *no* damage to the tritium target C1, and no ^{3}H contamination whatsoever.

The target was equipped with a variety of sensors (temperature, pressure, residual gas) all connected to 2 processors that continuously checked the status of the target, and relayed useful information to the data-acquisition computer. These independent processors had the responsibility to ensure proper operation of the target, and to stop the beam and close the transportation container in cases such as unexpected conditions, loss of integrity of the containers, power failure, failure of the processor units, etc.

As mentioned above, between container C3 and C4 there was another container TC. This "transportation container" had no windows, and was hermetically closed during all times when personnel was near the target. Only during operation of the target in the evacuated experimental hall HE1 could TC be opened by remote control. The pneumatic opening system included an air reservoir designed to close the container in case of power failure.

Use of a liquid target with minimized amounts of ^{3}H involves a large amount of heavy nuclei (Cu, Fe) near the beam. In order to avoid *all* background contributions, the beam was centered accurately on the target at all times, and it was tuned to have negligible halo (at r > 3 mm). A massive collimator made of uranium (diameter 8 mm) upstream of the target and outside the spectrometer acceptance, eliminated potential stray electrons. A secondary emission monitor upstream of the target verified that no beam-halo was present. The split secondary emission monitor described in the previous section ensured stabilization of the beam position to 0.1 mm accuracy.

For the extreme forward- and backward-angles of the 900 spectrometers (25° and 155°) the end caps of the target were not entirely outside the acceptance of the spectrometer. Insisting on this condition would have led to an undue increase of target length (i.e. quantity of ^{3}H). For the extreme angle of 155°—which is of great interest to the separation of F_{ch} and F_m — a special collimator was added

to the setup. This collimator at 155°, placed close to the ^{3}H target, eliminated all contributions from the end caps. It also led to a region of inaccessible angles between 110° and 150°, which did not impair the quality of the experimental results.

For the tritium experiment, we needed to accurately determine the target density, as we intended to measure *absolute* cross sections. The temperature and pressure of ^{3}H were measured with calibrated sensors, and continuously registered by the data acquisition computer during all runs. The liquid tritium pressure and temperature, LH_2 pressure and temperature, provided (under thermal equilibrium conditions) four independent measurements of the ^{3}H density, allowing to identify potential problems with time-dependent changes of calibrations, or inaccuracies during the initial calibration. The quantities required to determine the absolute density of the target at zero beam intensity are given in the reports of Roders *et al* [17], Souers *et al* [18] and Guizouarn [19]. At our nominal working temperature of 21.7K the target density was 0.2710±0.0014 g/cm^2. This led to a thickness of $\simeq$ 1 g/cm^2 at $\theta = 155°$.

The experiments on ^{3}He were performed with gaseous targets, with the ^{3}He at a temperature of 20K and a pressure of 12-14 bars. The ^{3}He was held in a vertical loop containing the target proper, a fan to circulate the gas and a heat exchanger made from grids of copper wire. These grids were anchored on a copper tube cooled by a bath of liquid hydrogen, furnished by a liquefying machine with a power of 50 W at 20 K. One of the targets is shown in Fig. 2, the other one was described in ref.[11]. These targets were equiped with various pressure and temperature sensors which were read out regularly during the experiment.

With this arrangement ^{3}He target densities of order 25 mg/cm^3 were achieved, yielding a useful thickness of 50 mg/cm^2 at $\vartheta = 155°$. The targets had stainless steel windows of 40 mg/cm^2 thickness, the target diameter being large enough to place the windows outside the spectrometer acceptance for all angles.

3 Experiments

3.1 Approach to L/T separation

The standard approach to determine charge and magnetic form factors individually is the one of the Rosenbluth separation. At constant momentum transfer q, the total form factor F is a linear function of $1/2 + tg^2\vartheta/2$, where ϑ is the scattering angle, *i.e.* $F^2(q) \simeq F_{ch}^2(q) + (1/2 + tg^2\vartheta/2) \cdot F_m^2(q)$. By a variation of the incident electron energy and ϑ, at constant q, this linear dependence can be mapped out. Measurement of the intercept and slope of a straight-line fit to the data on F^2 yields F_{ch} and F_m.

This procedure is straightforward conceptually, but extremely inefficient in practice. Every new ϑ for a given q requires a new incident electron energy, with a retuning of accelerator and switchyard. This is very time consuming. The safety considerations that apply when using a ^{3}H-target only compound this problem. Overall, this leads to experiments that measure a few values of q only, and provide a very limited set of data. A new set of experimental conditions for every data point also leads to different systematic errors; keeping track of them, and detecting their presence through systematics, becomes very intricate.

Moreover, data taking at "constant" q is rarely achieved in practice. Corrections to the energy (hence q) such as those due to energy loss in the target, or Coulomb corrections, then require non-transparent interpolation of the data.

For the present ^{3}H – experiment, we have chosen a novel approach. We have taken data at a few constant electron energies, but at *many* angles, covering at every energy the full angular range accessible by the spectrometer. As the spectrometer angle could be changed very quickly, an extensive set of data points could be measured, with systematic errors (such as normalization) common to all points. The form factors F_{ch} and F_m then could be extracted by a fit of the entire set of data at all E, ϑ, q with a flexible parametrization of $F_{ch}(q)$ and $F_m(q)$. Studies of this procedure before the experiment, carried out employing cross sections generated using Faddeev calculations, have demonstrated the efficiency and accuracy of this

approach.

This approach has a further advantage: for the nuclei ^{3}H and ^{3}He it is of great interest to separate the form factors into their isoscalar and isovector contributions. These are obtained from sums and differences of the ^{3}H and ^{3}He form factors. Such a separation becomes extremely limited in scope, and leads to large uncertainties of the result, if one can use only data from experiments that do achieve identical q-values for ^{3}H and ^{3}He. Extracting the form factors from a global fit to all available data, on the other hand, allows to determine with optimal accuracy the isoscalar and isovector form factors.

3.2 Data taking

Our first experiment on ^{3}He [11] was oriented towards a measurement of the ^{3}He magnetic form factor at large q. Accordingly, data were taken at a backward scattering angle of 155° and 13 different incident energies ranging from 300 to 700 MeV. These data extended the momentum transfer region up to 32 fm^{-2}. Forward angle data were taken at each energy for normalization purposes only.

In the second ^{3}He experiment we have accurately measured the charge form factor up to 24 fm^{-2}. These measurements were performed at an incident energy of 640 MeV and scattering angles between 35 and 123°. In order to improve the knowledge of the magnetic form factor around the diffraction minimum, magnetic cross sections at 155° and 7 energies between 315 and 415 MeV were measured as well.

In the tritium experiment both charge and magnetic form factors were measured. Data were taken at fifteen different energies from 190 to 685 MeV. For each energy we have measured an angular distribution at forward angles and a data point at 155°. The forward angle data were taken in order to determine the charge form factor, and also in order to allow a comparison between measurements at various energies.

An example of an experimental spectrum measured was already shown in figure

1. Using the reconstructed scattering angle and target coordinates, the raw spectrum was corrected for energy losses in the target before and after the scattering, and for kinematic broadening due to the finite angular acceptance. The central value of the peak channel corresponds to an electron that was scattered in the middle of the target and has the nominal scattering angle. The information on the energy of the peak, known precisely from the spectrometer energy calibration, plus corrections for recoil and energy losses in all target materials, allowed us to determine the incident energy. The energies listed in the tables are those recalculated for the incident electrons in the middle of the target, and are accurate to 2×10^{-4}.

Radiative effects

The experimental spectra were corrected for radiative effects using two different methods. In the first method the peak was integrated up to an excitation energy ΔE. The radiative correction factors were computed as a function of ΔE using the formulae of Mo and Tsai [20]; the Schwinger and bremsstrahlung effects were accounted for as well as Landau straggling in the target. In the second method, the radiative corrections were unfolded channel by channel by dividing the elastic peak area into a large number of channels of small width. The radiative tail was then computed for each channel separately, and subtracted from the spectrum at larger energy loss. This method allowed, in addition to the elastic peak, to compute the electrodisintegration cross sections. The two methods were found to agree to better than 1%.

In all three experiments we have made the attempt to determine as accurately as possible the various systematic effects affecting the determination of cross sections for ^{3}H (^{3}He), such as incident current, spectrometer extended target acceptance, spectrometer solid angle, target density and its dependence on the beam current and size, detector efficiency and dead time.

Integrated charge

The incident current was continuously checked by comparing the charge measured with the Faraday cup to the ones measured with the ferrite monitors. The ratio of these charges was constant within 1%. Effects of multiple scattering in the

target, leading to losses of the Faraday cup, were determined from Faraday/Ferrite ratios measured beforehand with targets of different thickness.

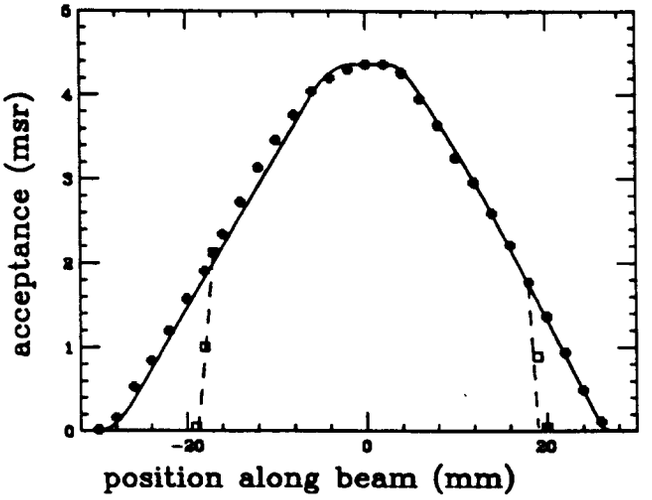

Figure 3: Acceptance of the spectrometer, measured with a thin target travelling along the beam. The square symbols correspond to the acceptance with the 155° collimator for the ^{3}H - target, the lines correspond to the acceptance calculated from geometry and the spectrometer field map.

Acceptance

The spectrometer acceptance for an extended target was measured with a thin ^{12}C target which was displaced along the beam. These measurements were performed both with and without the target collimators mentioned above. An example of such a measurement is shown in figure 3.

The accuracy of this measurement is 0.5%, and the measured acceptances agrees well with the ones calculated from the geometry of the slits and the known field maps of the spectrometer. The absolute overall solid angle for an extended target was then obtained from the solid angle at the center of the target — which is known with high accuracy as it depends on distance and area of the 900 spectrometer collimator only — and the relative solid angle measured by the travelling target. The resulting overall uncertainty on the spectrometer solid angles is better than 1%.

Target density variations

During all data taking periods, the dependence of the target density ρ on the incident beam intensity I was measured, at least once for each energy. When conserving nearly constant beam spot size, this local heating effect was found to amount to 1.2 $\%/\mu A$ for the liquid tritium target and 0.4 $\%/\mu A$ for the helium gas targets. The systematic error on $\rho(I)$ is 1% and 0.5% for the tritium and helium experiments, respectively.

For the two helium experiments the overall efficiency of the apparatus was calibrated using the forward angle cross sections between q^2 of 1 and 4 fm^{-2}, by comparing our data to the ones previously measured [10, 9, 6]. However, during the tritium experiment we have measured absolute cross sections. To achieve this, particular care was taken to measure the detection efficiency. This efficiency was obtained by exploiting the redundancy of the detector setup which had been complemented by an additional set of plastic detectors. The trigger efficiency was found to be 99$\pm$ 0.5 % and was constant during the experiment. The wire chamber efficiency was determined by computing the inefficiency of each plane separately (again exploiting the redundancy of the detector) and then combining the results. The overall efficiency was 93% $\pm$ 1%. A slight dependence on the beam intensity, due to the background coming from the target, was also found. This effect amounted to 0.1 $\%/\mu$A, and was accounted for in the determination of the cross section values.

Normalization error

All the various random errors were combined to a total random uncertainty of 1.5% – 3%, depending on the exact experiment. This overall random uncertainty was quadratically added to the statistical uncertainty of each data point. The final cross sections for all three experiments are listed in the tables 3,4 given in the appendix. The tritium data have in addition a systematic normalization uncertainty of 3%. For helium the forward-angle data have been normalized to the wellknown data at low momentum transfer; the corresponding normalization errors are not significant.

4 Data analysis

The cross sections measured in our experiments are presented in the tables in the appendix.

In order to analyze these data, we parametrize the various form factors using a flexible parametrization. From these form factors, we calculate cross sections including Coulomb corrections, and fit the parameters to the data. The separation of longitudinal and transverse form factors thereby is automatically achieved.

Sum-of-Gaussian parametrization

In order to fit the experimental, unseparated, data, we employ the Sum-of-Gaussians (SOG) parametrization [21] for $F_{ch}(q)$ and $F_m(q)$. The form factors are written as

$$F(q) = e^{-\frac{1}{2}q^2\gamma^2} \sum_{i=1}^{n} \frac{Q_i}{1+2R_i^2/\gamma^2} \left(cos(qR_i) + \frac{2R_i^2}{\gamma^2} \frac{sin(qR_i)}{qR_i} \right) \qquad (1)$$

For the present application only the q-space version is of interest *a priori*. In configuration space, this parametrization corresponds to a density $\rho(r)$ written as a sum of (symmetrized) gaussians that are placed at arbitrary radii R_i, with amplitudes Q_i that are fitted to the data, and a fixed width γ.

The choice of this parametrization is governed by the following considerations. To extract form factors not biased by the choice of the analytical form, we need a parametrization that in principle is totally general, with restrictions that can be justified on physical grounds. In the limit $\gamma \to 0, R_n \to \infty$ (hence $n \to \infty$) the SOG is a perfectly general basis. For a fit of the data, we introduce two restrictions:

1. The gaussians are given a finite width γ. In both $\rho_{ch}(r)$ and $\rho_m(r)$ we do not expect any structure that is smaller than allowed for by the proton size. Accordingly, we define γ via the rms-radius of the proton $\gamma\ \sqrt{3}/2 = 0.8fm$. This finite width essentially imposes that the form factors on average fall no slower than the proton form factor.

2. The gaussians are placed at radii $R_i \leq R_{max} = 5fm$. This is justified given

the fact that, from independent knowledge on the behaviour of wave functions at large radii, one can easily specify the radius at which the tails of densities give no significant ($< 10^{-3}$) contribution to $F(q)$. A finite R_{max} imposes that the form factor cannot oscillate in q-space more quickly than with a minimal wave length $\Delta q \propto 1/R_{max}$.

Both these restrictions have been tentatively relaxed during the analysis; we have found that this had a negligible effect on the form factors deduced.

The data have been fitted with the parametrization eq.(1), and 12 free parameters for each form factor. The data set for F_{ch} and F_m for ^{3}H and ^{3}He is thus fitted with 48 parameters.

Note that these form factors are simply used to parametrize the data; they are not the one-body form factors.

Error matrix

The statistical error of the fit is given by the error matrix E_{ij}. This quantity can also be used to calculate the error of any other quantity G(Q) that also depends on the Q_i, via

$$\delta G^2 = \sum_{ij} \frac{\partial G}{\partial Q_i} \frac{\partial G}{\partial Q_j} E_{ij}. \tag{2}$$

The systematic errors of the form factors have been evaluated by changing the individual data sets by their quoted error and refitting. The errors due to different, independent sets of data are added quadratically The total error is the quadratic sum of statistical and systematic errors.

Coulomb corrections

In order to analyze the electron scattering data we have assumed that the cross section can be expressed in the plane wave Born approximation (PWBA) as:

$$\frac{d\sigma}{d\Omega} = \left(\frac{d\sigma}{d\Omega}\right)_{Mott} \frac{1}{\eta} \left[\frac{q^2}{\vec{q}^2} F_{ch}^2(q) + \frac{\mu^2 q^2}{2M^2} \left(\frac{1}{2}\frac{q^2}{\vec{q}^2} + tan^2\frac{\vartheta}{2}\right) F_m^2(q)\right] \tag{3}$$

where the Mott cross section contains the usual recoil and Z^2 factors, μ is the

^{3}H (^{3}He) magnetic moment, η is given by $(1 + q^2/4M_T^2)$. M (M_T) is the nucleon (three-nucleon) mass and q $(\vec{q})$ is the four (three)-momentum transfer.

This equation is not entirely correct in practice. The incident electron wave is distorted by the Coulomb field of the nucleus. As a consequence the PWBA is not entirely valid, and form factors defined as the ratio of experimental to Mott cross sections would not depend on the momentum transfer q^2 alone, but also on the incident energy E and angle ϑ. The DWBA form factors $F^2_{ch,DW}(E,\vartheta)$ and $F^2_{m,DW}(E,\vartheta)$ are related to the Born form factors $F^2_{ch}(q)$ and $F^2_m(q)$ by:

$$F^2_{ch}(q) = F^2_{ch,DW}(E,\vartheta) f_c(E,\vartheta) \tag{4}$$

and

$$F^2_m(q) = F^2_{m,DW}(E,\vartheta) f_m(E,\vartheta) \tag{5}$$

where f_{ch} and f_m are Coulomb correction factors. Unfolding of these corrections allows to restore the PWBA formula and to infer the PWBA form factors that can be compared to theoretical predictions and will be used throughout this paper.

In order to unfold the Coulomb corrections from the experimental cross sections we have applied the following procedure. First we have made fits to the data assuming that PWBA is valid. This allowed us to derive approximate charge and magnetisation densities which were then used to compute the cross sections as a function of the actual energies and angles. This was done using a phase shift code for charge scattering, and the DWBA code HADES [22] for magnetic scattering. The Coulomb correction factors (eqs.4,5) were then obtained from the ratio of the exact to the PWBA cross sections. The Coulomb corrections were found to be insensitive to the exact densities employed.

5 Experimental form factors

In order to provide the most complete experimental information on the A=3 form factors, we give in this paper only the results obtained by analysing our new data *together* with *all* the data for A=3 previously measured.

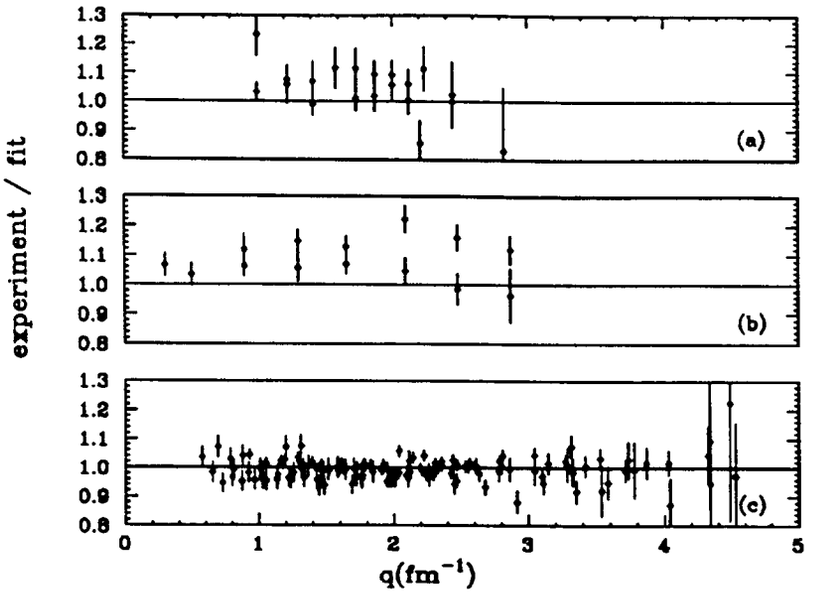

Figure 4: Ratio of the experimental ^{3}H cross sections to fit, for the data of Collard *et al(a), Beck* et al(b), and the present experiment (c).

For the fits we use cross sections when available, and we have calculated the corresponding Coulomb corrections; otherwise, we use the form factors that have been extracted. In the fits we include the full set of data of refs. [5, 6, 8, 7, 10, 11, 12] [9, 13, 14]. The fits were limited to the region $q^2 \leq 35 fm^{-2}$ where the set of data is reasonably complete. Higher-q data are available for (mainly charge) scattering from ^{3}He [7].

For ^{3}H we have a total of 190 data points, and the total χ^2 amounts to 340. This χ^2 is obtained when using the statistical errors of the data only. The highest χ^2 per data point comes from the data of [13], which, as shown by figure 4, are too high by about 8%.

For ^{3}He we use a total of 280 data points, and the total χ^2 amounts to 326. The deviations of individual data sets from the fit is shown in figure 5. Again, we show only the lower-q data, *i.e.* the range where systematic (normalization) differences could be important.

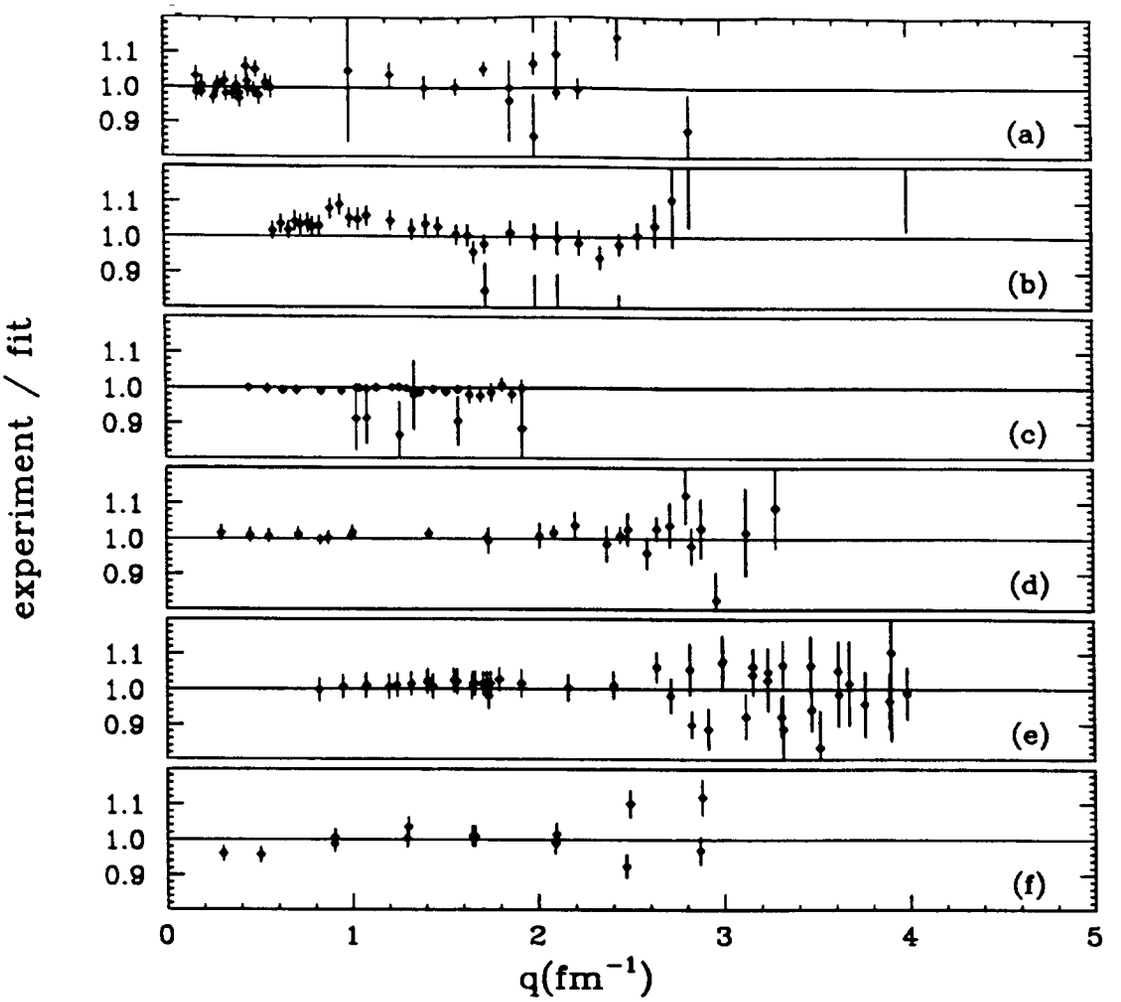

Figure 5: Ratio of the experimental cross sections to fit, for the ^{3}He data of Collard *et al* (and Szalata *et al* at low q) (a), McCarthy *et al* (b), Ottermann *et al* (c), Dunn *et al* (d), the present experiment (e), and Beck *et al* (f).

We have tentatively renormalized those data sets that show noticeable systematic deviations, and have found that these renormalizations do not in a significant way influence the fit results. We therefore have kept the original data as published, at the expense of a somewhat larger χ^2 ; we believe, however, that for a set of data as varied as the one for ^{3}He , taken over an interval of 30 years, the agreement – when taking into account the published systematic uncertainties — is quite satisfactory.

The results of our fits are quoted in table 1 in terms of the *SOG* parameters for the four form factors. The uncertainties of the extracted values, including the

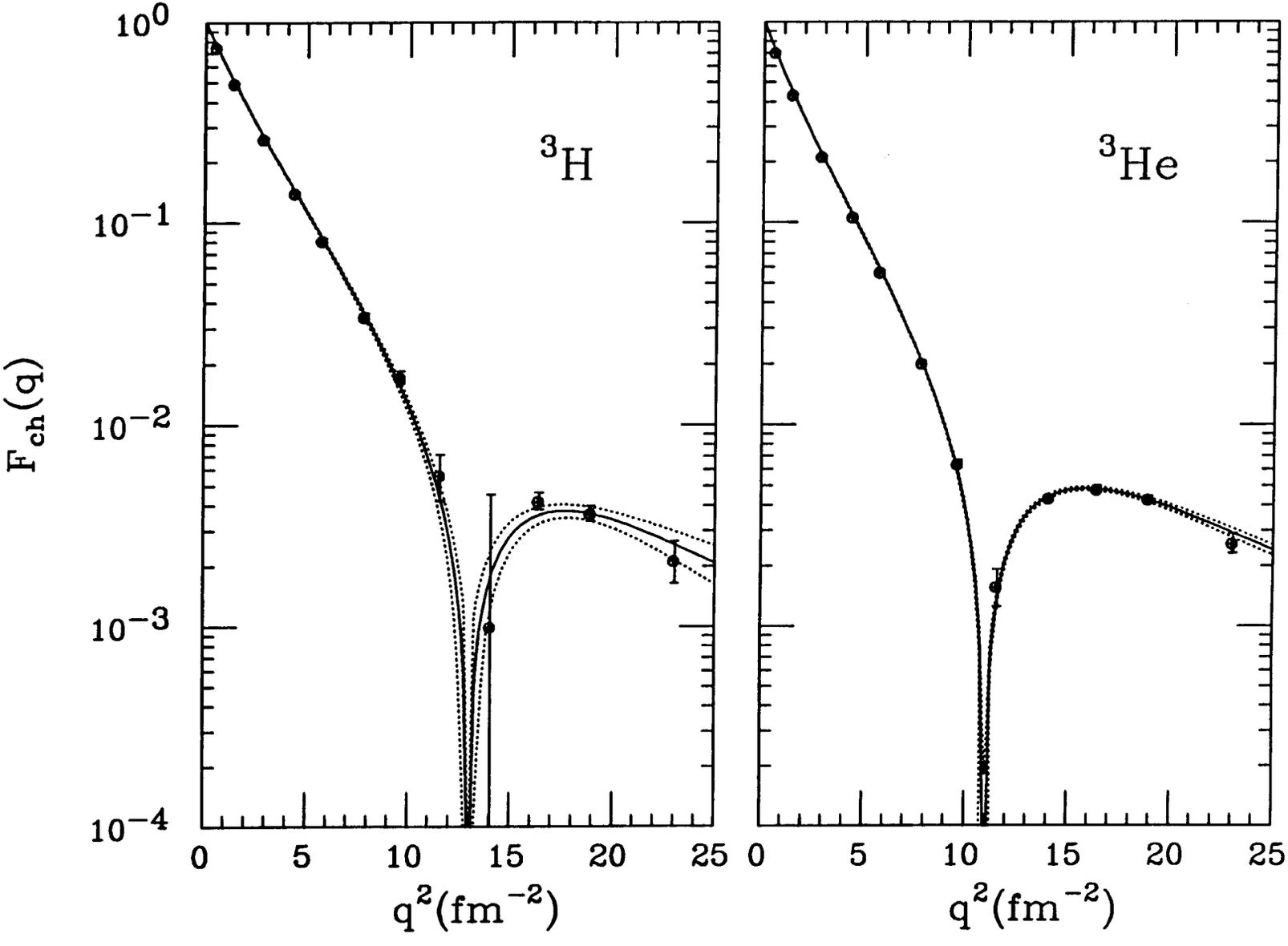

Figure 6: Best fit charge form factor for ^{3}H (solid line) with limits of error band. (dashed). The points correspond to values extracted via the usual Rosenbluth technique

Figure 7: Same as for figure 6, but for ^{3}He.

R_i	Q_i^c ^{3}H	Q_i^m ^{3}H	Q_i^c ^{3}He	Q_i^m ^{3}He
0.1	0.054706	0.075234	0.027614	0.059785
0.5	0.172505	0.164700	0.170847	0.138368
0.9	0.313852	0.273033	0.219805	0.281326
1.3	0.072056	0.037591	0.170486	0.000037
1.6	0.225333	0.252089	0.134453	0.289808
2.0	0.020849	0.027036	0.100953	0.019056
2.4	0.097374	0.098445	0.074310	0.114825
2.9	0.022273	0.040160	0.053970	0.042296
3.4	0.011933	0.016696	0.023689	0.028345
4.0	0.009121	0.015077	0.017502	0.018312
4.6	0.000000	0.000000	0.002034	0.007843
5.2	0.000000	0.000000	0.004338	0.000000

Table 1: SOG parameters for ^{3}H and ^{3}He charge and magnetic form factors. The radii R_i are given in fm, the rms-radius of the gaussians is $0.8fm$.

systematic errors, are given in the figures 6,7,8,9 for the form factors, and can be read off with more precision from figure 10.

The parametrization of the ^{3}He charge and magnetic form factors is valid up to 35 fm^{-2}. The ^{3}H charge form factor is well determined up to 25 fm^{-2}, the magnetic form factor up to 31 fm^{-2}. At larger q^2 the values determined by the fit to the data still have finite error bars, but the values are essentially determined from the extrapolation inherent in the parametrization.

We have also performed standard Rosenbluth separations of the data. When forward- and backward-angle data are not exactly at the same momentum transfer, we use the fit to shift the data to the q-value desired. This is done by using at the q-value of interest the same ratio $\sigma_{exp}/\sigma_{fit}$ as at the neighbouring experimental q-value. The resulting F_{ch} and F_m agree with the ones from the global fit, and are also shown in the figures.

The error bars of the Rosenbluth-separated form factors are less precise, however, as for a determination at a given q the global fit *de facto* uses the values of all data in the neighbouring q-interval; the width of this interval is given by $\sim 1/R_{max} \simeq$

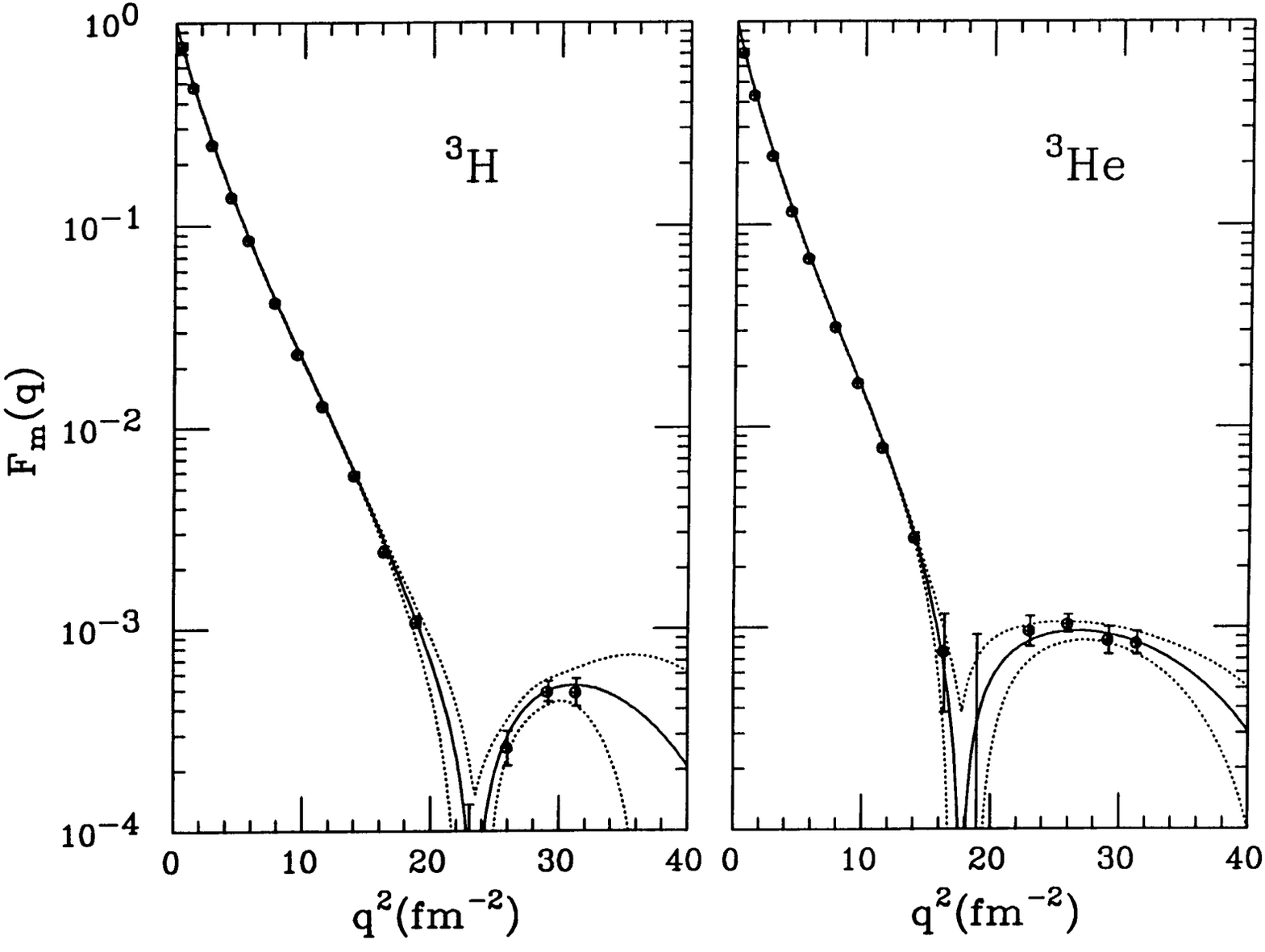

Figure 8: Best fit magnetic form factor for ^{3}H (solid line) with limits of error band. (dashed). The points correspond to values extracted via the usual Rosenbluth technique

Figure 9: Same as for figure 8, but for ^{3}He.

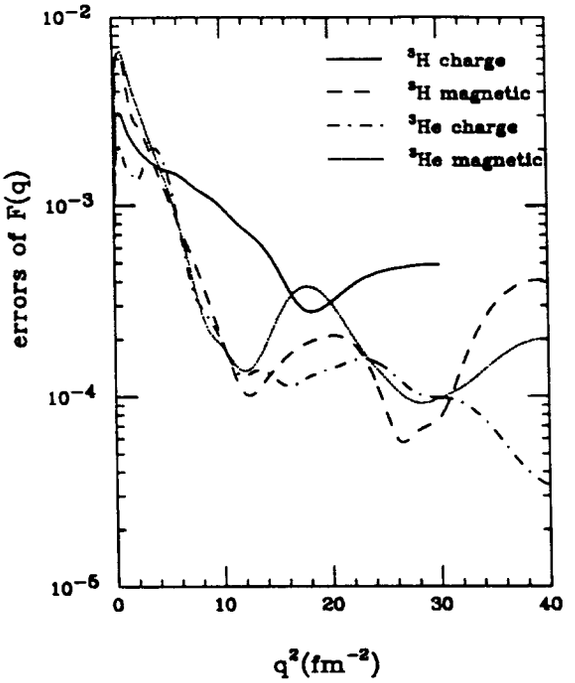

Figure 10: Uncertainty of the four form factors, covering both statistical and systematic errors of the data.

$0.2fm^{-1}$.

We emphasize that the *fit* of the data, together with its *error band*, is the quantity that contains the *full information* on the data for the A=3 system. These quantities should be used when comparing theory and experiment. Admittedly, this representation of the "data" is unconventional. However, for the reasons explained above, we conclude that it is the best way to summarize the full experimental information contained in the multitude of experimental results for ^{3}H and ^{3}He.

For some applications it also might be interesting to extract the best slopes of the form factors at $q^2 = 0$. We quote these slopes in table 2 in terms of the conventional "rms-radii", without further discussion. We note that the values simply correspond to the slopes; only to the degree that MEC can be ignored can these values be taken as genuine radii.

r_{ch} ^{3}H	r_m ^{3}H	r_{ch} ^{3}He	r_m ^{3}He
1.755	1.840	1.959	1.965
$\pm$ 0.086	$\pm$ 0.181	$\pm$ 0.030	$\pm$ 0.153

Table 2: Charge and magnetic rms radii and uncertainties for ^{3}H and ^{3}He in units of fm. The error bars cover both the statistical and the systenatic uncertainties.

6 Comparison with theory

In this chapter we compare our results with selected theoretical calculations. It is beyond the scope of this paper to give an extensive comparison to the theoretical predictions available. Here we restrict the comparison to theory to some of the most complete calculations. We only try to give a representative image of the present agreement or the remaining differences between calculation and data.

We take advantage of the fact that all trinucleon form factors are now accurately known up to momentum transfers of around 25 fm^{-2} to make simultaneous comparison with theory for both the ^{3}He and ^{3}H form factors. As explained above, the data are always shown as best fit values with the corresponding error bars.

In the comparison with theory we use the calculations of ref.[2, 23] and ref.[24, 25], which are based on nucleonic degrees of freedom. In both calculations the meson exchange currents (MEC) and the three-body force are included. Furthermore all the trinucleon form factors have been calculated in a consistent way.

Sauer and collaborators [2, 23] solve the coupled-channel Faddeev equations in momentum space, and use the Paris NN potential modified[2] to include Δ-isobar excitations via π- and ρ-meson exchanges. The presence of the Δ thus accounts for the most important part of the three-body force. In this calculation π-, ρ-, and $\rho\gamma\pi$-meson exchange current contributions are included as well as the one-body Darwin-Foldy and spin-orbit relativistic corrections.

Schiavilla and collaborators [24, 25] base their calculation on a variational three-body wave function computed using the Argonne V_{14} interaction and the Urbana-

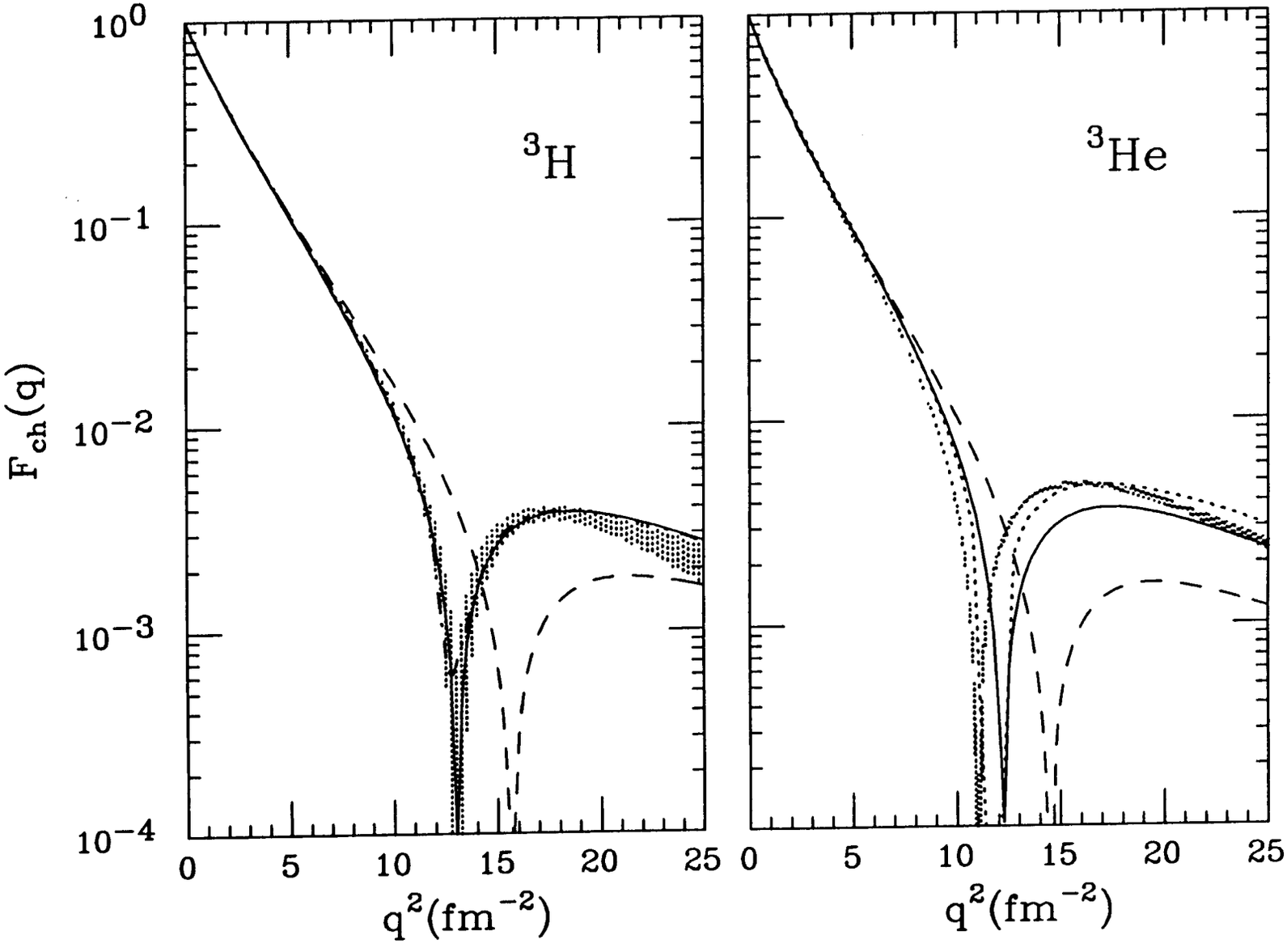

Figure 11: Data for charge form factor for ^{3}H with calculations of Sauer *et al* (solid) and Schiavilla *et al* (dotted). The IA of Sauer *et al* is shown as a dashed line

Figure 12: Same as for figure 11, but for ^{3}He.

VII three-nucleon force. In this calculation the π-like and ρ-like meson exchange currents are derived consistently from the NN interaction used. The authors also include the one-body relativistic corrections mentioned above as well as ω-exchange and $\omega\gamma\rho$-contributions.

6.1 Charge form factors

In figures 11,12 the data are compared to the calculations of refs.[23, 25]. For both calculations the MEC and relativistic corrections significantly displace the diffraction minimum to lower q values and increase the height of the secondary maximum by more than a factor of two. The two calculations achieve a similarly good agreement with ^{3}H. This is not the case for ^{3}He where ref.[23] slightly underestimates the form factor, whereas the calculation of ref.[24] almost perfectly agrees with it. The difference could be due to the model dependence of the one-body term, or due to different two-body contributions. Indeed, for the ^{3}H form factor, the calculations of refs.[23] and [25] predict the one-body minimum at 15.8 and 17.3 fm^{-2} respectively, while the predictions for the total form factor perfectly agree. Additional differences might come from the different parametrizations of the nucleon form factors used, particularly for the poorly known G_{en}. We do not understand why the ^{3}H form factors are better predicted than the ones for ^{3}He .

Calculations of the trinucleon charge form factors have also been carried out by Lina and Goulard [27]. Similar agreement with the data was obtained. In all these studies the π and ρ two-body contributions were found to be significantly larger (roughly a factor of 10) than the one-body relativistic corrections. More recently the relativistic effects in the trinucleon were investigated in a consistent manner by Rupp and Tjon[28]. They have found that, in addition to an increase of the triton binding energy by 0.3-0.4 MeV, the relativistic treatment tends to produce a diffraction minimum at somewhat larger momentum transfer.

A large effort has been devoted in the last decade to reproduce the triton binding energy. It was shown by several authors [1, 4] that its experimental value can be reproduced by adding three-body forces. A question then naturally arises: what is

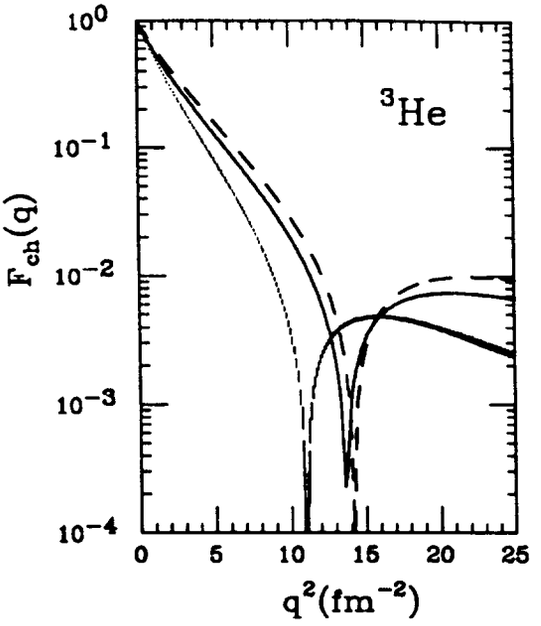

Figure 13: Effect of the three-body force [26] on the charge form factor. The solid curve is the prediction of the impulse approximation, the dashed curve takes into account the three-body force. The calculations do not include MEC's, while the data (shaded area) do.

the *specific* effect of the three-body force on the three-nucleon form factors? Friar *et al* [26] have studied the A = 3 charge form factors using several two-body models and three-body forces in a Faddeev calculation. A typical calculation which uses a three-body force is shown in Fig.13. While the three-body force significantly modifies the binding energy, its effect on the charge form factors is quite small. To achieve agreement with the form factor data, relativistic effects and the contribution of MEC's, which are more important, have to be added.

6.2 Magnetic form factors

The data for the ^{3}He and ^{3}H magnetic form factors are displayed in figures 14,15. They are of comparable accuracy and extend to the same momentum transfer. While the effect of the three-body force is also quite small, the effect of the meson-exchange

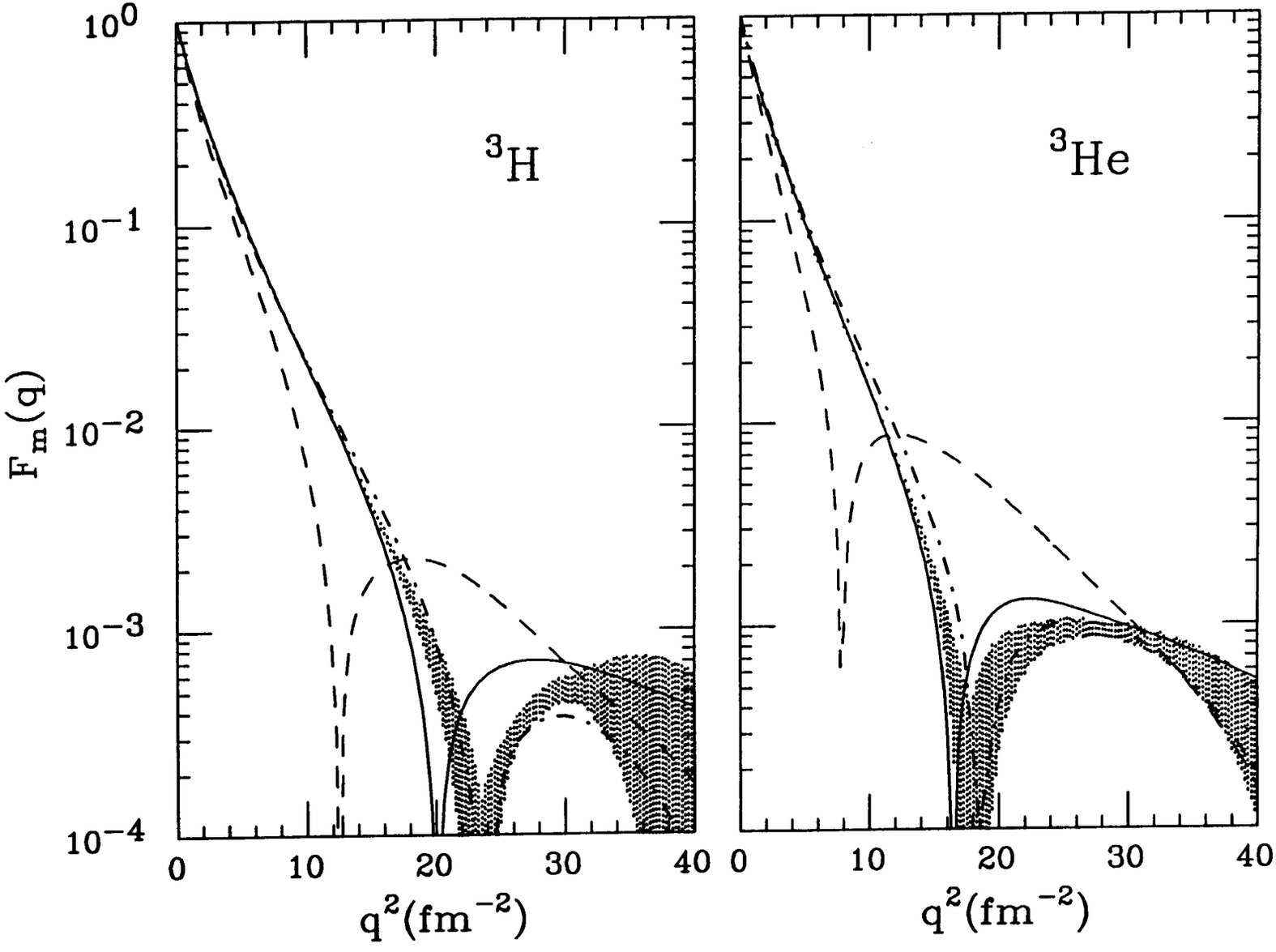

Figure 14: Data for magnetic form factor for ^{3}H with calculations of Sauer *et al* (solid) and Schiavilla *et al* (dotted). The IA of Sauer *et al* is shown as a dashed line.

Figure 15: Same as for figure 14, but for ^{3}He.

currents is larger than for the charge form factors. Figures 14,15 show the two full calculations [23, 24], in one case we also show the IA result. The destructive interference of the contributions of the S–S and S–D transitions results in a one-body diffraction minimum which is far away from the experimental one. Meson exchange currents improve considerably the agreement with the experiment. However, none of the calculations perfectly accounts for the shape of the ^{3}He form factor: the prediction of ref.[2] explains its shape below the diffraction minimum, but fails above, whereas ref.[24] shows the opposite behaviour. The latter calculation agrees with the ^{3}H form factor, while this is not the case for ref.[2].

There are several differences between these two calculations. As for the charge form factors they differently predict the one-body contribution. The IA predictions for the location of the diffraction minima of ^{3}H are 12.5 and 13.8 fm^{-2} for the calculations of Sauer and Schiavilla, respectively. The differences in the exchange current contribution are even larger. They come first from the pion-like pseudoscalar component of the potential. This term is stronger for the calculation of ref.[24] than for the calculation of ref.[2]. In addition, in the expression of the two-body operators, the authors of ref.[24] use the G_e nucleon electromagnetic form factor whereas the good agreement with the data for [2] is obtained when using the F_1 form factor. The effect of chosing different nucleon form factors and vertex form factors was recently discussed in ref.[29].

While qualitatively the role of MEC is understood, the situation for the magnetic form factors in particular is not yet satisfactory when it comes to a quantitative comparison.

7 Isoscalar-isovector form factors

We have previously published [14] a separation of the A=3 form factors. Here, we present the final results, based on the set of world data.

The isoscalar $F_{T=0}$ and isovector $F_{T=1}$ components of the A = 3 form factors are defined by the following expressions:

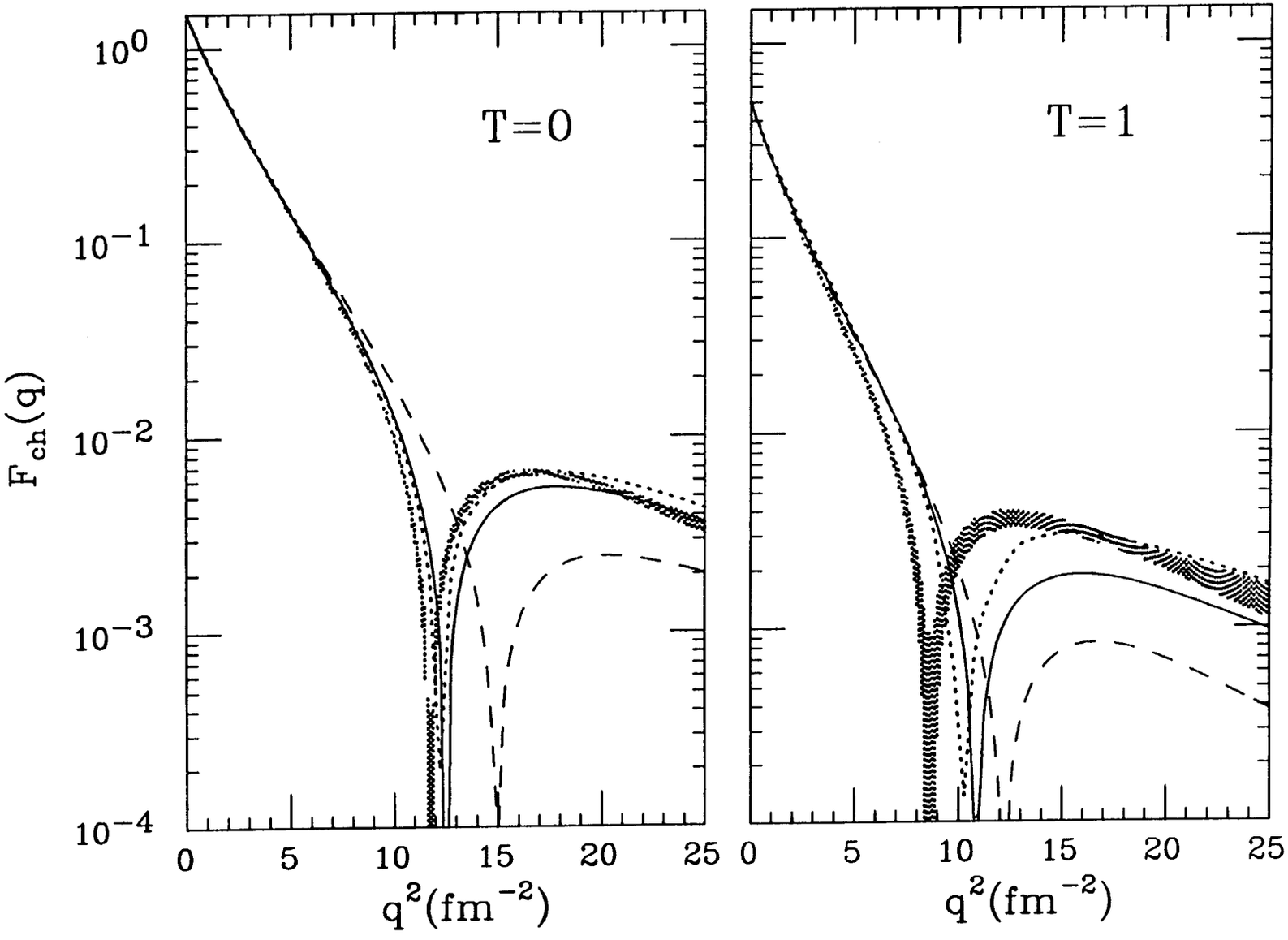

Figure 16: Data for T=0 charge form factor with calculations of Sauer *et al* (solid) and Schiavilla *et al* (dotted). The IA of Sauer *et al* is shown as a dashed line.

Figure 17: Same as for figure 16, but for T=1.

$$F_0(q) = \frac{1}{2}\left[2F_{He}(q) + F_H(q)\right] \tag{6}$$

$$F_1(q) = \frac{1}{2}\left[2F_{He}(q) - F_H(q)\right] \tag{7}$$

and similarly for the magnetic form factors:

$$F_0(q) = \frac{1}{2}\left[\mu_{He}F_{He}(q) + \mu_H F_H(q)\right] \tag{8}$$

$$F_1(q) = \frac{1}{2}\left[\mu_{He}F_{He}(q) - \mu_H F_H(q)\right] \tag{9}$$

where μ_H and μ_{He} are the A=3 magnetic moments and all ^{3}He /^{3}H form factors are normalized to 1 at $q = 0$. The T=0,1 form factors can easily be calculated from the parameters given in table 1, by taking the same linear combinations of the Q_i as shown in *eqs* 6-9. The effect of the isospin impurity, due to the Coulomb interaction in ^{3}He, has been neglected. Indeed, its effect on the ^{3}He charge form factor is very small, $\leq 1\%$ in the region of the secondary diffraction maximum and even smaller for lower q values.

Figures 16,17 and 18,19 show the separated $A = 3$ form factors together with the theoretical predictions of refs.[23, 25]. The main observations from these comparisons are:

1) The T=0 charge form factor is remarkably well predicted by both calculations. This agreement is quite unexpected since it is reached after adding two-body meson-exchange contributions, which lead to a sizeable change. As stated above, they are of relativistic order and thus model dependent.

2) For the T = 1 charge form factor we observe large differences between the theoretical predictions. Moreover, none of them perfectly describes the data. Since the agreement for the T =0 component has been found to be excellent for all of them, we conclude that improvement in the description of the trinucleon requires improvement of the calculation of its isovector charge component.

3) For the T=0 magnetic form factor the two calculations show the same results below 15 fm^{-2}, but qualitatively differ beyond. The contribution of the T=0 meson-exchange currents is negligible. This observation would indicate that the trinucleon

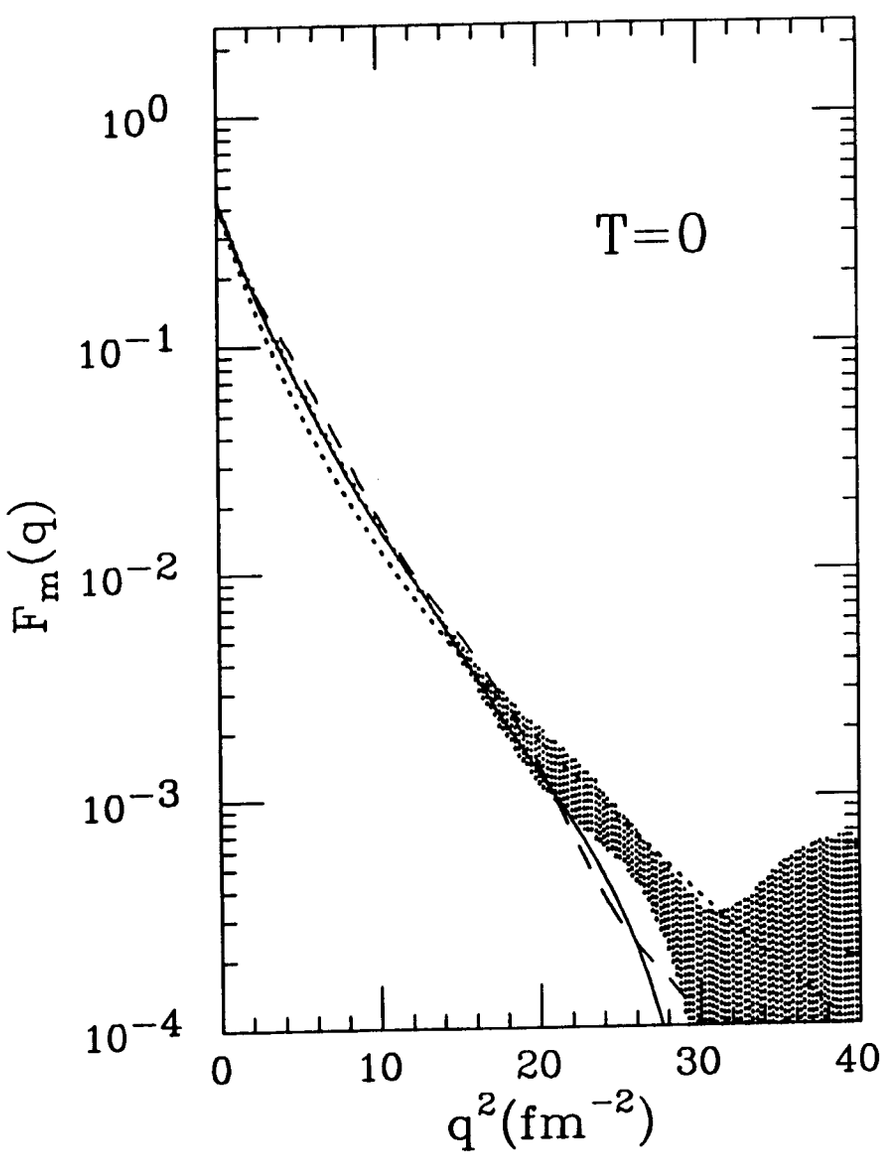

Figure 18: Data for T=0 magnetic form factor with calculations of Sauer *et al* (solid) and Schiavilla *et al* (dotted). The IA of Sauer *et al* is shown as a dashed line.

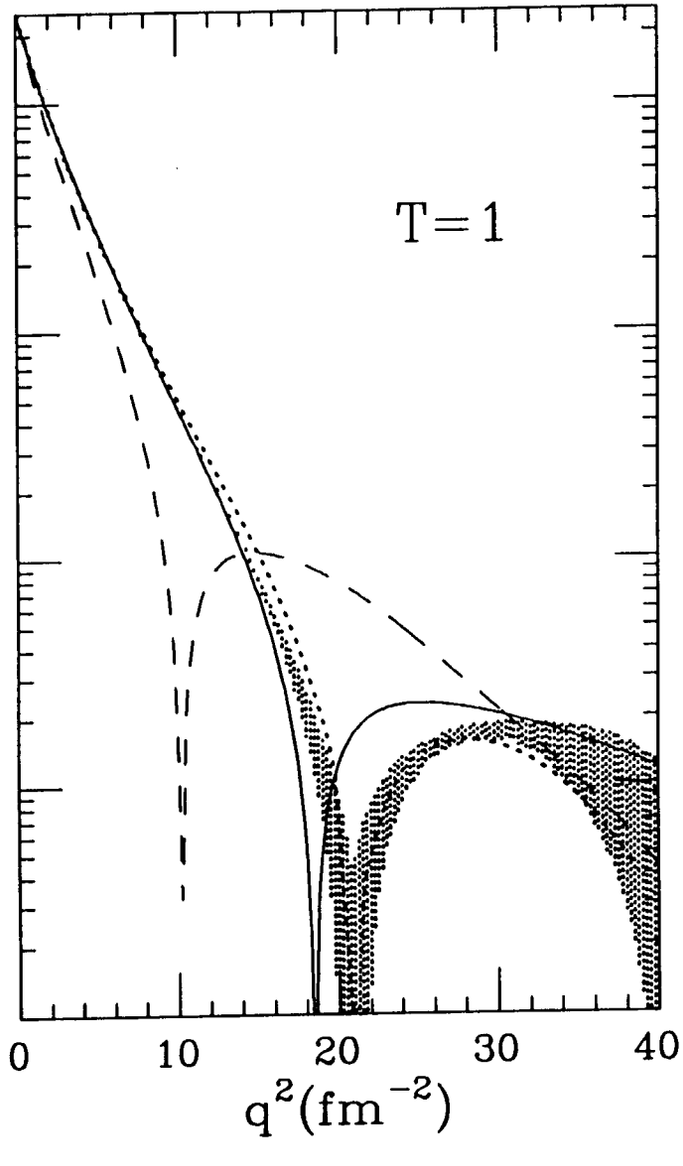

Figure 19: Same as for figure 18, but for T=1.

wave function is well described by calculations up to about 15 fm^{-2}, but remains more uncertain beyond. The discussion of the ^{3}He and ^{3}H form factor above has also shown that the discrepancies in the one-body contributions obtained with different nucleon-nucleon models are still large in the region of the secondary diffraction maximum.

4) Reasonable agreement between theory and data is observed also for the T = 1 magnetic form factor. The behaviour of the theoretical curves is quite similar to the one obtained for ^{3}He and ^{3}H form factors. The small differences between the two calculations reflect larger, but partly cancelling, variations in the one- and two-body contributions as discussed above.

7.1 Comparison to A=2,4 nuclei

The trinucleon isoscalar charge form factor contains the same two-body exchange charge operators as those occuring in the charge form factors of the deuteron and of ^4He. Figure 20 shows the data for these nuclei, together with the theoretical predictions of [30] for the deuteron and of [25] for ^4He. For all A = 2, 3 and 4 nuclei the corrections beyond IA include the Darwin-Foldy and spin-orbit relativistic corrections, and π-, ρ- and $\rho\gamma\pi$ exchange current operators. It is clearly seen from the figure that the three nuclei exhibit similar diffraction structure. The position of the experimental diffraction minima, which reflect the increasing size and more rapid falloff of the density in the surface region, are located near 20, 12 and 10 fm^{-2} for A = 2, 3 and 4 nuclei, respectively. For all three form factors IA alone predicts a minimum at too large values of q, and significantly underestimates the form factors in the region of the secondary diffraction maximum. The inclusion of one-body relativistic corrections and two-body meson-exchange currents improves the agreement between experiment and theory, but does not entirely explain the experimental data.

The two- and three-nucleon isoscalar charge form factors have recently been studied by Henning et al.[29] with the same nucleon-nucleon interaction (the Paris potential) and meson-exchange contributions. They have investigated the influence

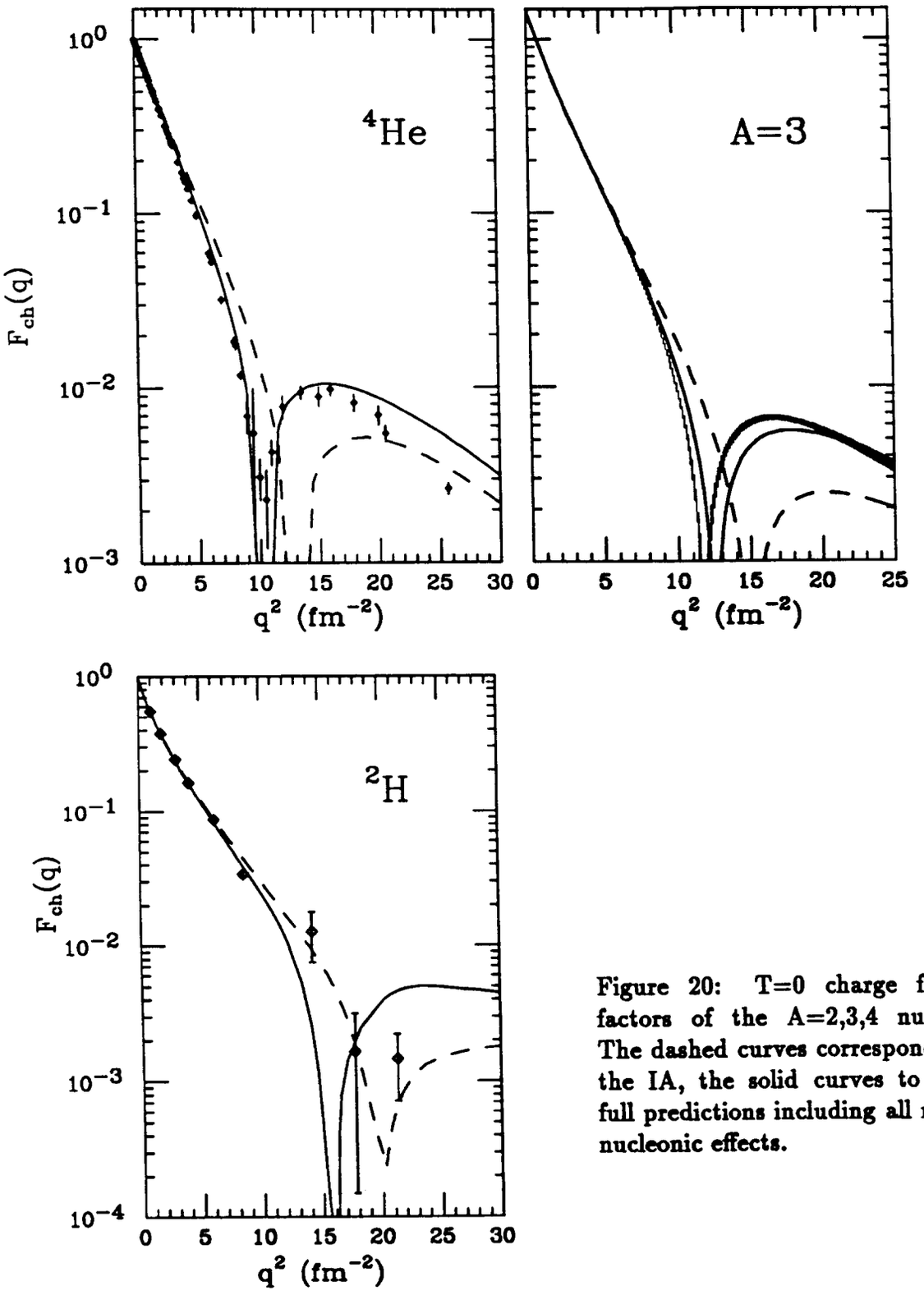

Figure 20: T=0 charge form factors of the A=2,3,4 nuclei. The dashed curves correspond to the IA, the solid curves to the full predictions including all non-nucleonic effects.

of the nucleon electromagnetic form factors and the strength of the π-pair term.

They conclude that if the calculation is modified in order to fit the deuteron data, the good agreement with the trinucleon is destroyed, and vice versa. Thus present calculations are not yet able to simultaneously explain the data for the A=2,3,4 nuclei with a consistent description in terms of nucleonic and non-nucleonic degrees of freedom.

Figure 21 compares the trinucleon isovector magnetic form factor with the cross

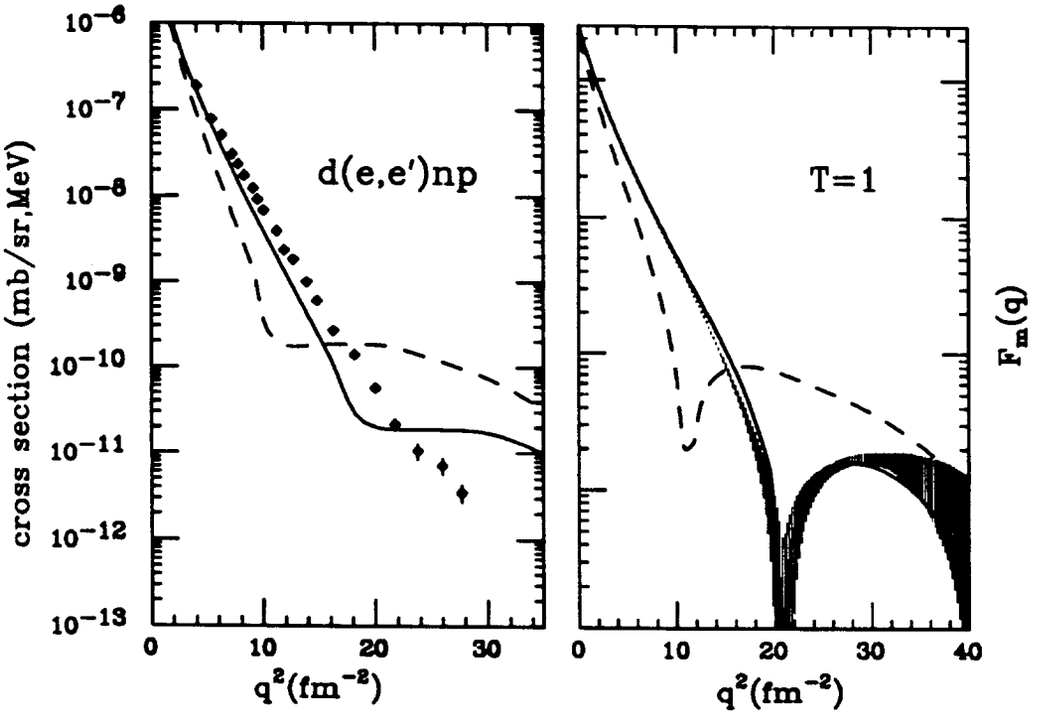

Figure 21: T=1 magnetic cross sections (form factors) for the A=2,3 systems. The dashed curves correspond to the IA, the solid curves to the full predictions including all non-nucleonic effects.

section for electrodisintegration of the deuteron at threshold [31, 32, 33]. The experimental diffraction minimum is located near 20 fm^{-2} in the three-nucleon system; the corresponding minimum for the deuteron is probably located near 25 fm^{-2}. It has not been yet been observed [32, 33]; in deuteron electrodisintegration M1 is not the only multipolarity, due to the finite experimental resolution higher multipolarities also contribute to the cross section. The calculations used are from refs.[24, 25] for

the trinucleon and [30] for the deuteron. For both nuclei the nucleonic contribution to the cross section has a diffraction zero at a relatively small momentum transfer due to the destructive interference between the one-body S–S and S–D amplitudes. Inclusion of the same two-body currents leads to similarly good agreement between experiment and theory. This agreement clearly confirms the well known importance of the contribution of meson-exchange currents in the T = 1 magnetic transitions. Contrary to expectations, however, their contribution is of similar importance for F_m and for F_{ch}, and the degree to which data can be explained by theory is not better for magnetic transitions, even though meson exchange currents there are first order corrections.

8 Conclusions

In this paper we have presented the results from three successive experiments on electron scattering from ^{3}H and ^{3}He. The measurements greatly extend the range of momentum transfer of the ^{3}H data, and significantly improve the precision for the data already available for ^{3}He.

From these data, combined with the complete set of world data, we have extracted the ^{3}H and ^{3}He charge and magnetic form factors up to momentum transfers of 30 fm^{-2}. In order to extract these observables in an optimal way, the form factors were determined via a fit to *all* data simultaneously.

The three-nucleon form factors are now well determined in the q-range where their description in terms of nucleons and meson exchange currents is valid. The detailed comparison with theory shows good agreement with experiment. To obtain this good agreement, it is necessary to both perform calculations of the three-body wave functions corresponding to the solution of the Schrödinger equation for a realistic N–N potential, and to include the contributions of meson-exchange currents. Small differences, particularly at the higher momentum transfers, remain. The might be due to relativistic effects, which were found to be important in the A=2 system, bur are poorly known for A=3.

The A=2,4 form factors essentially contains the same physics as the A= 3 isoscalar and isovector form factors. The comparison between experiment and theory shows similar overall agreement. The remaining differences observed for the A=2,3,4 nuclei do not have a clear interpretation. Changes in the input of theoretical calculations, such as vertex form factors, that improve the agreement for one nucleus often cause a degradation for another one.

Further progress in the experimental study of the 3-body system will require higher momentum transfer data which can be measured at CEBAF. This will lead to better spatial resolution and an enhancement of non-nucleonic over nucleonic contributions. This will allow one to address the question of the understanding of ^{3}H and ^{3}He in terms of the fundamental constituents, quarks and gluons. Such an understanding is the challenge for the future.

9 Acknowledgements

Two laboratories from the Commissariat à l'Energie Atomique at Saclay and Bruyères le Châtel have joined their efforts for the success of this work. The use of a liquid ^{3}H target in an intense electron beam required an extraordinary effort of the DPHN/HE laboratory as a whole, and the series of experiments described in this paper would not have been possible without the help of many people. We would like to thank in particular R. Delsaut, J. Dupont, A. Godin, B. Hervieu, M. Hirq, M. Maurier, and J.C. Zerbib.

References

[1] C.R. Chen, G.L. Payne, J.L. Friar, and B.F. Gibson. *Phys.Rev.Lett.*, 55:374, 1985.

[2] Ch. Hajduk, P.U. Sauer, and W. Strueve. *Nucl. Phys.*, A405:581, 1983.

[3] R. Schiavilla, V.R. Pandharipande, and R.B. Wiringa. *Nucl.Phys.*, A449:219, 1986.

[4] T. Sasakawa and S. Ishikawa. *Few Body Syst.*, 1:3, 1986.

[5] H. Collard, R. Hofstadter, E.B. Hughes, A. Johanson, M.R. Yearian, R.B. Day, and R.T. Wagner. *Phys. Rev.*, C15:B57, 1965.

[6] J.S. McCarthy, I. Sick, and R.R. Whitney. *Phys.Rev.*, C15:1396, 1977.

[7] R.G. Arnold, B.T. Chertok, S. Rock, W.P. Schuetz, Z.M. Szalata, D. Day, J.S. Mc Carthy, F. Martin, B.A. Mecking, I. Sick, and G. Tamas. *Phys. Rev. Lett.*, 40:1429, 1978.

[8] Z.M. Szalata, J.M. Finn, J. Flanz, F. J. Kline, G.A.Peterson, J.W. Lightbody Jr., X.K. Maruyama, and S. Penner. *Phys.Rev. C*, 15:1200, 1977.

[9] C.R Ottermann, G. Koebschall, K. Maure, K. Roehrich, Ch. Schmitt, and V.H. Walther. *Nucl. Phys.*, A435:688, 1985.

[10] P.C. Dunn, S.B. Kowalski, F.N. Rad, C.P. Sargent, W.E. Turchinetz, R. Goloskie, and D.P. Saylor. *Phys. Rev.*, C27:71, 1983.

[11] J.M. Cavedon, B. Frois, D. Goutte, M. Huet, Ph. Leconte, C.N. Papanicolas, X.-H. Phan, S.K. Platchkov, S. Williamson, W. Boeglin, and I. Sick. *Phys. Rev. Lett.*, 49:978, 1982.

[12] F.P. Juster, S. Auffret, J.-M. Cavedon, J.-C. Clemens, B. Frois, D. Goutte, M. Huet, P. Leconte, J. Martino, Y. Mizuno, X.-H. Phan, S. Platchkov, S. Williamson, and I. Sick. *Phys.Rev.Lett.*, 55:2261, 1985.

[13] D. Beck, A. Bernstein, I. Blomqvist, H. Caplan, D. Day, P. Demos, W. Dodge, G. Dodson, K. Dow, S. Dytman, M. Farkhondeh, J. Flanz an K. Giovanetti, R. Goloskie, E. Hallin, E. Knill, S. Kowalski, J. Lightbody, R. Lindgren, X. Maruyama, J. McCarthy, B. Quinn, G. Retzlaff, W. Sapp, C. Sargent, D. Skopik, I. The, D. Tieger, W. Turchinetz, T. Ueng, N. Videla, K. von Reden, R. Whitney, D. Skopik, and C. Williamson. *Phys.Rev. Lett.*, 59:1537, 1987.

[14] A.Amroun, V. Breton, J.-M. Cavedon, B. Frois, D. Goutte, J. Martino, X.-H. Phan, S.K. Platchkov, I. Sick, and S. Williamson. *Phys.Rev.Lett.*, 69:253, 1992.

[15] P. Leconte, J. Mougey, A. Tomasso, P. Barreau, M. Bernheim, A. Bussiere de Nercy, L. Cohen, J.-C. Comoretto, J. Dupont, S. Frullani, C. Grunberg, J.-M .Hisleur, J. Le Devehat, M. Lefevre, G.Lemarchand, J. Millaud, D. Royer, and R. Salvaudon. *Nucl. Instr. and Meth.*, 169:401, 1979.

[16] W. Bertozzi and. *Nucl. Instr. and Methods*, 141:457, 1977.

[17] H.M. Roder *et al. U.S. National Bureau of Standards*, Technical Report NBS-641, 1973.

[18] P.C. Souers. *Lawrence Livermore Lab.*, Rep. UCRL-52628, 1973.

[19] L. Gouizouarn. *Comm.En.Atom., CEN Grenoble*, Rep. CENG/ASP:65–11, 1965.

[20] L.W. Mo and Y.S. Tsai. *Rev. Mod. Phys*, 46:815, 1969.

[21] I. Sick. *Nucl.Phys.*, A218:509, 1974.

[22] H. Andresen. *priv. com.*

[23] W. Strueve, Ch. Hajduk, P.U. Sauer, and W. Theis. *Nucl. Phys.*, A465:651, 1987.

[24] R. Schiavilla, V.R. Pandharipande, and D.O Riska. *Phys.Rev.C*, 40:2294, 1989.

[25] R. Schiavilla, V.R. Pandharipande, and D.O. Riska. *Phys.Rev.C*, 41:309, 1990.

[26] J.L. Friar, B.F. Gibson, and G.L. Payne. *Phys.Rev.*, C35:1502, 1987.

[27] J.M. Lina and B. Goulard. *Phys.Rev.*, C34:714, 1986.

[28] G. Rupp and J.A. Tjon. *Phys.Rev.*, C45:2133, 1992.

[29] H. Henning, J.Adam, and P.U. Sauer. *Few Body Syst.*, Suppl.5:133, 1992.

[30] R. Schiavilla and D.O. Riska. *Phys. Rev.*, C43:437, 1991.

[31] S. Auffret, J.-M. Cavedon, J.-Clemens, B. Frois, D. Goutte, M. Huet, F.P. Juster, P. Leconte, J. Martino, Y. Mizuno, X.H. Phan, S. Platchkov, and I. Sick. *Phys. Rev. Lett.*, 55:1362, 1985.

[32] P.E. Bosted, A.T. Katramatou, R.G.Arnold, D. Benton, L. Clogher, G. DeChambrier, J. Lambert, A. Lung, G.G. Petratos, A. Rahbar, S.E. Rock, Z.M. Szalata, D.Debebe, M. Frodyma, R.S. Hicks, A. Hotta, G.A. Peterson, R.A. Gearhart, J. Alster, J. Lichtenstadt, F. Dietrich, and K. VanBibber. *Phys.Rev.*, C42:38, 1990.

[33] K.S. Lee, W. Schmitt, H. Baghaei, D. Beck, P. Bosted, S. Chruchwell, B. Frois, R.S. Hicks, A.Hotta, J. Martino, R.A. Miskimen, G. Peterson, S.K. Platchkov, M. Spengo, W. Turchinetz, K. Wang, C.F. Williamson, JT. Yates, and J.D. Zumbro. *Phys.Rev.Lett.*, 67:2634, 1991.

10 Appendix

Table 3: Cross sections for ^3He. The notation $1.234 - 5$ stands for $(1.234 \cdot 10^{-5})$ mb/sr.

energy	angle	cross section	error	energy	angle	cross section	error
MeV	degrees	mb/sr	%	MeV	degrees	mb/sr	%
314.4	30.0	$1.923 - 2$	3.3	640.0	45.0	$6.769 - 6$	3.8
	35.0	$7.973 - 3$	3.2		50.0	$1.510 - 6$	3.9
	40.0	$3.486 - 3$	3.3		54.0	$4.244 - 7$	6.8
	45.0	$1.581 - 3$	3.3		58.0	$1.116 - 7$	7.2
	50.0	$7.511 - 4$	3.3		62.0	$2.792 - 8$	4.8
	55.0	$3.622 - 4$	3.3		64.0	$1.476 - 8$	6.4
	60.0	$1.835 - 4$	3.2		66.0	$9.059 - 9$	6.4
	155.0	$3.401 - 8$	4.1		70.0	$4.876 - 9$	6.5
335.4	50.0	$5.232 - 4$	3.2		74.0	$4.403 - 9$	9.1
	60.0	$1.174 - 4$	3.2		78.0	$3.735 - 9$	9.5
	155.0	$1.652 - 8$	5.0		82.0	$3.091 - 9$	8.1
	60.0	$7.754 - 5$	3.1		85.0	$2.623 - 9$	7.3
	155.0	$7.340 - 9$	5.4		94.0	$1.290 - 9$	8.4
365.2	55.0	$1.379 - 4$	3.2		102.0	$7.627 - 10$	13.9
	155.0	$4.869 - 9$	8.5		112.0	$2.780 - 10$	15.1
374.3	55.0	$1.155 - 4$	3.2		123.0	$8.129 - 11$	29.7
	155.0	$3.294 - 9$	6.0	300.5	155.0	$5.518 - 8$	4.9
394.5	50.0	$1.825 - 4$	3.4	325.5	155.0	$1.974 - 8$	6.4
	53.0	$1.057 - 4$	3.4	350.5	155.0	$7.869 - 9$	6.9
	55.0	$7.871 - 5$	3.1	375.5	155.0	$2.759 - 9$	10.4
	155.0	$1.479 - 9$	7.7	400.5	155.0	$8.906 - 10$	12.5
413.3	30.0	$6.547 - 3$	3.2	421.0	155.0	$4.450 - 10$	11.7
	35.0	$2.314 - 3$	3.3	450.5	155.0	$1.594 - 10$	22.7
	40.0	$8.687 - 4$	3.2	514.0	155.0	$5.185 - 11$	30.4
	45.0	$3.336 - 4$	3.5	568.5	155.0	$3.225 - 11$	41.0
	50.0	$1.320 - 4$	3.2	585.0	155.0	$5.978 - 11$	24.5
	155.0	$6.422 - 10$	7.8	603.9	155.0	$6.319 - 11$	21.6
640.0	35.0	$1.292 - 4$	3.7	629.5	155.0	$2.578 - 11$	33.5
	40.0	$2.953 - 5$	3.7	659.5	155.0	$2.302 - 11$	33.5
				688.9	155.0	$1.936 - 11$	30.4

Table 4: Cross sections for ^3H. The notation $1.234 - 5$ stands for $(1.234 \cdot 10^{-5})$ mb/sr. A 3% systematic error has to be added.

energy	angle	cross section	error	energy	angle	cross section	error
189.2	35.0	1.194 − 2	3.5	269.2	155.0	4.390 − 7	3.5
	40.0	6.030 − 3	3.4	308.8	35.0	2.790 − 3	1.5
	45.0	3.262 − 3	3.4		40.0	1.269 − 3	1.6
	50.0	1.958 − 3	3.5		45.0	6.233 − 4	1.6
	55.0	1.169 − 3	3.5		50.0	3.218 − 4	1.6
	65.0	4.900 − 4	3.4		55.0	1.674 − 4	1.5
	80.0	1.585 − 4	3.5		60.0	8.999 − 5	1.6
	85.0	1.013 − 4	3.4		65.0	5.045 − 5	1.6
	90.0	7.870 − 5	3.5		82.0	8.308 − 6	3.4
	95.0	5.325 − 5	3.4		90.0	4.019 − 6	3.4
	155.0	4.462 − 6	3.5		100.0	1.798 − 6	3.5
229.2	35.0	7.327 − 3	3.4		155.0	1.335 − 7	3.4
	40.0	3.604 − 3	3.4	348.6	35.0	1.730 − 3	1.6
	45.0	1.968 − 3	3.5		40.0	7.782 − 4	1.7
	50.0	1.018 − 3	3.5		45.0	3.497 − 4	1.6
	55.0	5.927 − 4	3.5		50.0	1.700 − 4	1.6
	60.0	3.625 − 4	3.5		55.0	8.518 − 5	1.6
	65.0	2.207 − 4	3.4		60.0	4.432 − 5	1.8
	82.0	5.146 − 5	3.4		65.0	2.362 − 5	1.6
	85.0	4.104 − 5	3.5		82.0	3.428 − 6	1.7
	90.0	2.842 − 5	3.4		90.0	1.585 − 6	1.8
	95.0	1.982 − 5	3.4		100.0	6.536 − 7	1.8
	100.0	1.428 − 5	3.4		155.0	3.679 − 8	2.0
	155.0	1.548 − 6	3.5	388.6	35.0	1.123 − 3	1.7
269.2	35.0	4.179 − 3	3.5		40.0	4.662 − 4	1.7
	40.0	2.032 − 3	3.4		50.0	9.251 − 5	1.6
	45.0	1.025 − 3	3.4		55.0	4.314 − 5	1.8
	50.0	5.510 − 4	3.5		60.0	2.149 − 5	1.6
	55.0	3.068 − 4	3.4		65.0	1.074 − 5	1.8
	60.0	1.762 − 4	3.4		82.0	1.351 − 6	1.7
	65.0	1.027 − 4	3.4		90.0	5.731 − 7	2.5
	66.0	9.083 − 5	3.5		100.0	2.208 − 7	2.6
	68.0	7.417 − 5	3.4		155.0	9.761 − 9	3.5
	80.0	2.389 − 5	3.4	428.6	35.0	7.300 − 4	1.6
	82.0	2.068 − 5	3.5		40.0	2.837 − 4	1.6
	90.0	1.079 − 5	3.5		45.0	1.175 − 4	1.7
	100.0	5.034 − 6	3.4		50.0	5.071 − 5	1.7
269.2	102.0	4.394 − 6	3.5	428.6	55.0	2.137 − 5	1.8

Table 4: continuation

energy MeV	angle degrees	cross section mb/sr	error %	energy MeV	angle degrees	cross section mb/sr	error %
428.6	60.0	1.012 – 5	1.5	538.6	30.0	6.671 – 4	1.6
428.6	65.0	4.820 – 6	1.8		35.0	2.116 – 4	1.8
428.6	82.0	4.765 – 7	2.6		40.0	7.060 – 5	1.8
428.6	90.0	2.006 – 7	3.8		45.0	2.394 – 5	1.6
428.6	99.0	7.798 – 8	4.8		50.0	8.709 – 6	1.6
428.6	155.0	2.224 – 9	6.1		55.0	3.247 – 6	1.7
468.7	40.0	1.712 – 4	1.8		60.0	1.283 – 6	1.7
468.7	45.0	6.717 – 5	1.7		65.0	5.258 – 7	1.9
468.7	50.0	2.693 – 5	1.8		82.0	3.350 – 8	3.5
468.7	55.0	1.120 – 5	1.7		90.0	9.029 – 9	9.4
468.7	60.0	4.832 – 6	1.7		100.0	2.678 – 9	9.6
468.7	65.0	2.267 – 6	1.9		155.0	1.702 – 11	62.9
468.7	82.0	1.665 – 7	4.2	569.0	45.0	1.626 – 5	1.8
468.7	90.0	6.526 – 8	3.6		50.0	5.494 – 6	1.5
468.7	100.0	2.200 – 8	4.8		155.0	1.782 – 12	82.5
468.7	155.0	3.602 – 10	10.2	619.0	45.0	7.404 – 6	1.5
508.4	30.0	8.670 – 4	1.5		50.0	2.347 – 6	1.6
508.4	40.0	1.030 – 4	1.5		68.0	4.930 – 8	5.7
508.4	45.0	3.752 – 5	1.6		80.0	5.104 – 9	3.6
508.4	50.0	1.440 – 5	1.5		85.0	2.384 – 9	5.1
508.4	54.0	6.789 – 6	1.6		153.6	8.749 – 12	50.0
508.4	55.0	5.630 – 6	1.6		155.0	7.335 – 12	31.5
508.4	60.0	2.328 – 6	1.6	658.9	40.0	1.512 – 5	1.8
508.4	155.0	6.751 – 11	23.2		45.0	4.109 – 6	1.5
508.4	40.0	1.031 – 4	1.6		83.0	1.296 – 9	4.1
508.4	45.0	3.820 – 5	1.6		92.5	3.749 – 10	9.6
508.4	50.0	1.420 – 5	1.6		100.0	1.414 – 10	18.7
508.4	55.0	5.536 – 6	1.8		155.0	1.351 – 11	35.5
508.4	60.0	2.202 – 6	2.4	683.7	35.0	4.244 – 5	1.8
508.4	65.0	9.513 – 7	2.5		40.0	1.054 – 5	1.6
508.4	82.0	6.949 – 8	3.5		45.0	2.814 – 6	1.5
508.4	90.0	2.114 – 8	4.1		50.0	7.933 – 7	1.8
508.4	100.0	6.417 – 9	5.7		55.0	2.275 – 7	2.5
508.4	155.0	7.831 – 11	21.4		60.0	6.653 – 8	2.1
528.9	45.0	2.772 – 5	1.7		66.0	1.703 – 8	3.2
528.9	50.0	1.036 – 5	1.5		155.0	1.185 – 11	51.8
528.9	155.0	3.366 – 11	33.3	683.7	104.0	5.600 – 11	50.0